Gondwana Research 111 (2022) 249–264

Contents lists available at ScienceDirect

Gondwana Research

journal homepage: www.elsevier.com/locate/gr

Contrasting thermal evolution of the West African Equatorial and Central Atlantic continental margins

M. Wildman [a,*], R. Brown [a,†], J. Ye [b,c], D. Chardon [b], D. Rouby [b], A.N. Kouamelan [d], M. Dall'Asta [e]

[a] School of Geographical and Earth Sciences, College of Science and Engineering, University of Glasgow, Gregory Building, Glasgow G12 8RZ, Scotland
[b] GET, Université de Toulouse, CNRS, IRD, UPS, CNES, Toulouse, France
[c] Ali I. Al-Naimi Petroleum Engineering Research Center, King Abdullah University of Science & Techonology, Thuwal 23955-6900, Saudi Arabia
[d] UFR STRM, Université Houphouët-Boigny, Abidjan-Cocody, 22 B.P. 582 Abidjan 22, Cote d'Ivoire
[e] Total Energies R&D, CSTJF Av. Larribau, 64018 Pau Cedex, France

ARTICLE INFO

Article history:
Received 1 December 2021
Revised 28 July 2022
Accepted 17 August 2022
Available online 23 August 2022
Handling Editor: T. Gerya

Keywords:
Thermochronology
Apatite fission-track
Transform Margin
Tectonics
West Africa

ABSTRACT

The landscape of the West African continental margins is the product of tectonic, thermal and surface processes acting in concert during and following the breakup of Gondwana. Central Atlantic opening was marked by the emplacement of the Central Atlantic Magmatic Province (CAMP) and continental breakup proceeded through Late Jurassic and Early Cretaceous divergent tectonics while opening of the Equatorial Atlantic was dominated by early and mid-Cretaceous transform movement. The onshore erosional response to these events is poorly constrained yet is a crucial component of our understanding of topographic evolution and sediment transfer across continental margins. We present new apatite fission-track (AFT) data for 24 samples from Guinea and 11 samples from Ivory Coast, and thermal histories from inverse modelling. Our data and thermal histories show the following: the thermal effect of the CAMP across Guinea and Ivory Coast; rapid cooling along the coast during the early to mid-Cretaceous related to erosion of short-wavelength rift-shoulders; moderate cooling across longer wavelengths reflecting a pattern of erosion across flexural margin upwarps; and low cooling rates from the start of the Cenozoic to present day, consistent with low magnitudes of erosion inferred by onshore geomorphological data. We present our results alongside the published regional AFT dataset and draw inferences on the thermal and tectonic evolution of the onshore margin.

1. Introduction

Divergent margins are first-order features of global plate tectonics. Constraining the erosional history across the onshore domain of these margins is critical for understanding the response of the Earth's surface to tectonic and climatic processes over million-year timescales (Summerfield, 2000; Séranne and Anka, 2005). The Guinean-Ivory Coast sector of the West African continental margins (Fig. 1) presents a complex case-study due to the multi-phase history of rifting and interaction of a predominantly Jurassic extensional system in the Central Atlantic along the northern Guinean margin (Biari et al., 2017) and an Early Cretaceous transform dominated system in the Equatorial Atlantic along the Ivory Coast margin (Basile et al., 2005).

Advances in understanding rifting chronology and the development of offshore sedimentary basins along the margins has revealed links between the margins' tectonic and geodynamic evolution and vertical motions (i.e., uplift and subsidence) across both the onshore and offshore domains (Attoh et al., 2004; Burke and Gunnell, 2008; Grimaud et al., 2018; Ye et al., 2019). Recent work involving mapping of dated lateritic palaeo-landforms (e.g., Beauvais and Chardon, 2013; Grimaud et al., 2014; Chardon et al., 2016) and inverting river profiles (Lodhia et al., 2019) has revealed very low magnitude denudation and spatially variable uplift from ca. 45 Ma and has been interpreted within the context of basin-and-swell mantle driven uplift, long-term sea-level fall, and climate changes during this time. This data has been linked to offshore sediment accumulation data to constrain source-to-sink relationships across the margin during the Cenozoic (Grimaud et al., 2018; Lodhia et al., 2019). However, the paucity of onshore Mesozoic geological markers means that the tectonic and geomorphic evolution of West Africa from the onset of Central

* Corresponding author.
E-mail address: mark.wildman@glasgow.ac.uk (M. Wildman).
† Deceased.

https://doi.org/10.1016/j.gr.2022.08.010
1342-937X/

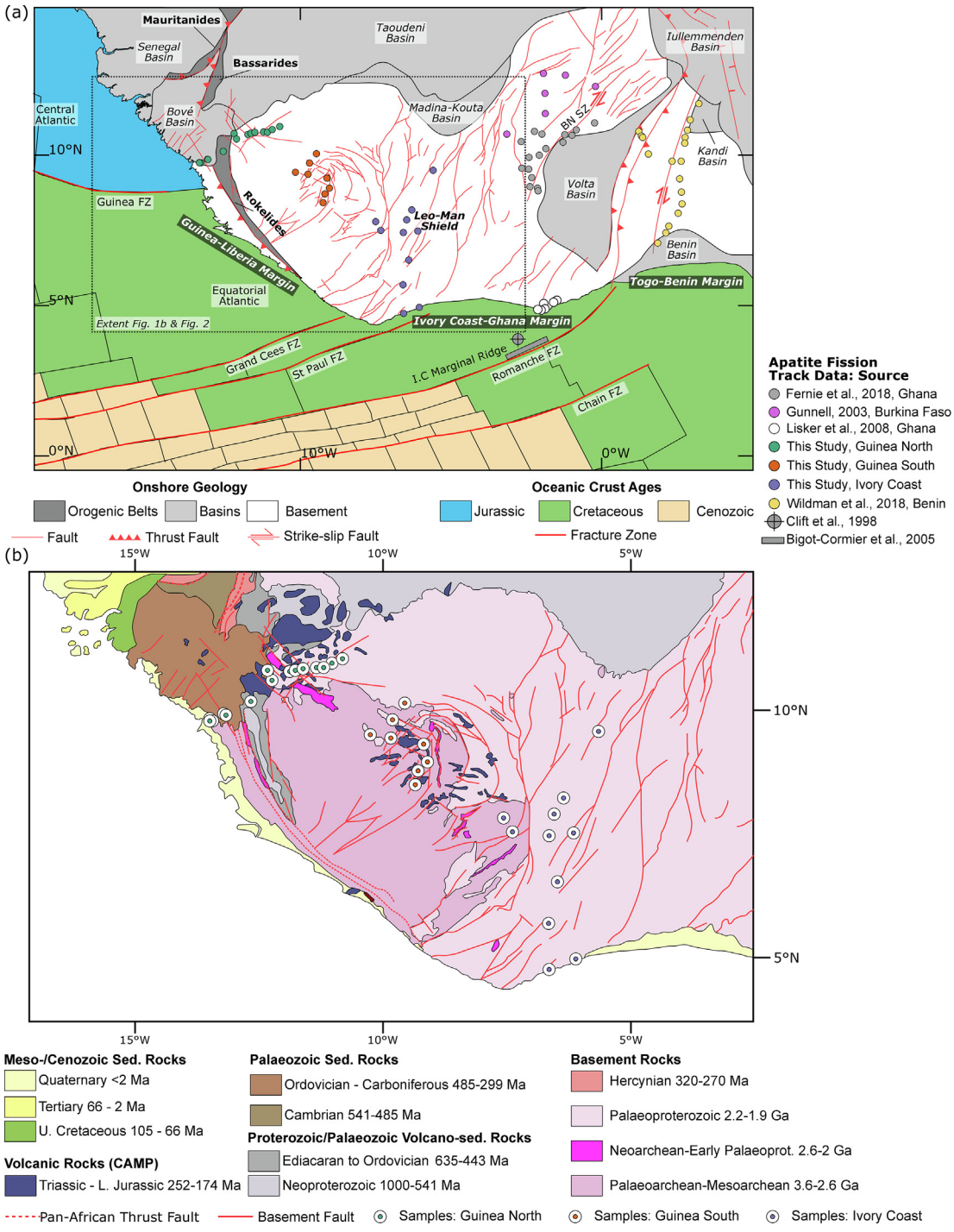

Fig. 1. (a) Tectonic map of West Africa showing major sedimentary basins, deformation belts, faults and Leo-Man cratonic shield onshore and major fracture zones (FZ) and oceanic crust age offshore. BN SZ – Bole Nangodi shear zone. Location of apatite fission-track data, colour coded for their publication are shown. (b) Geology of part of the map area of Fig. 1a showing the location of the samples from Guinea and Ivory Coast presented in this study.

Atlantic rifting in the late Jurassic (Labails et al., 2010) to the Cenozoic remains poorly understood. Moreover, there remains a lack of thermochronological data that, in the absence of these markers, can provide insights into periods of thermal or tectonic activity, enhanced erosion, and/or burial by constraining rock thermal histories.

The apatite fission-track (AFT) thermochronometer has been used globally to constrain denudation and burial along continental margins (see Wildman et al., 2020 for a review) by providing data on the timing and rate of rock cooling. Apatite fission-track data in West Africa has been limited to onshore studies in Burkina Faso (Gunnell, 2003), Ghana (Lisker et al., 2008; Fernie et al., 2018), Benin (Wildman et al., 2019), and from offshore wells along a marginal ridge in the Ivory Coast Basin (Clift et al., 1998; Bigot-Cormier et al., 2005). We present new AFT data from Guinea and Ivory Coast (Fig. 1b, Fig. 2) and obtain thermal histories for these regions using Bayesian inverse modelling to investigate the thermal response of the upper crust along the Guinean and Ivory Coast margin segments in response to superimposed rifting. We also discuss our data alongside previously published AFT datasets from West Africa

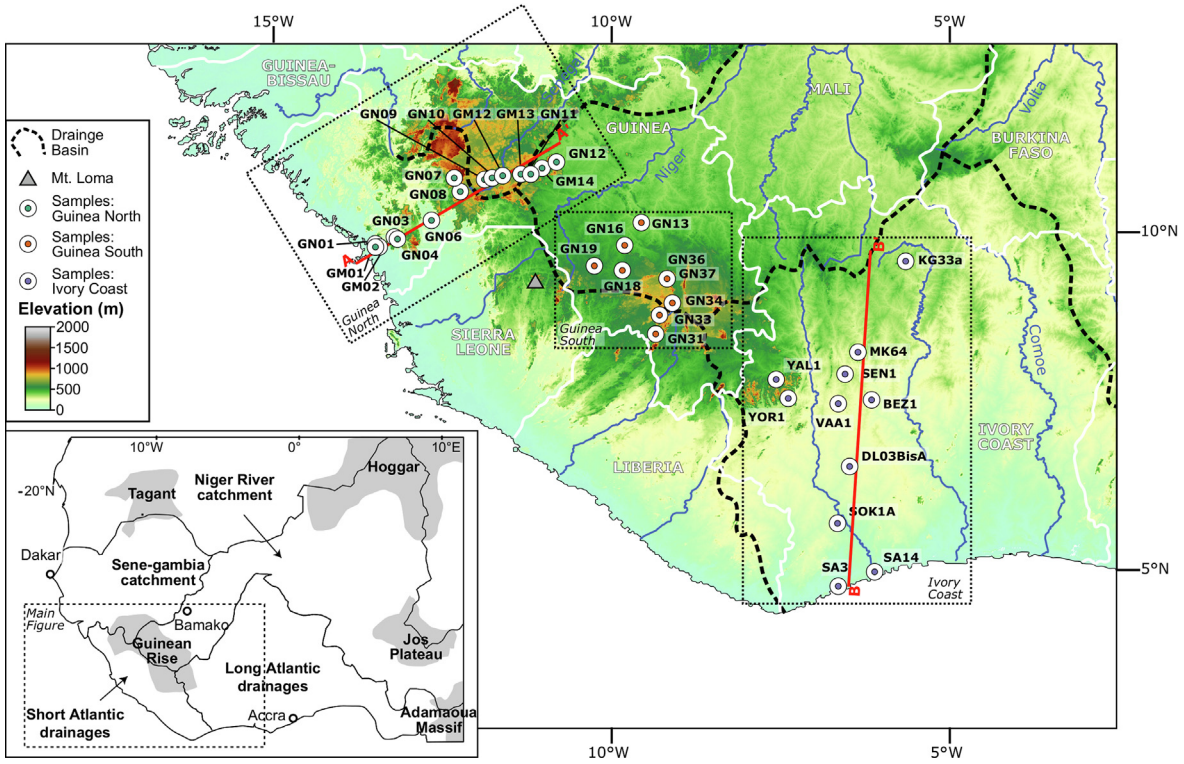

Fig. 2. Topographic map of the Guinea-Ivory Coast region of West Africa showing major rivers and drainage divides, sample locations and lines of transects shown in Fig. 5 and Fig. 6. Inset figure shows West African drainage patterns after Grimaud et al. (2018) and major elevated topographic features.

to draw more regional conclusions on the tectonic evolution of the region.

2. West African geological setting

2.1. Summary of rifting and break-up along the West African margin

The West African continental margin is segmented by transform faults with the extensional Central Atlantic Ocean segment North of the Guinea fracture zone (FZ) (Biari et al., 2017) (Fig. 1a). The Guinea-Liberia margin, Ivory Coast-Ghana margin and Togo-Benin sub-margins are transtensional systems creating pull-apart oblique normal faults, splay faults, and step-over and extensional duplex structures (Nemcok et al. 2016) bounded by the major St. Paul FZ, Romanche FZ and Chain FZ transform faults, respectively (Ye et al., 2017, 2019; Basile et al., 2005; Basile, 2015; Moulin et al., 2010; Heine et al., 2013). Transpressional structures have also been mapped in offshore Ghana and Ivory Coast (Tari, 2006). The structural variations across each of these segments and the onshore and offshore geological record are testament to the prolonged and multi-phase history of rifting (Ye et al., 2017, 2019).

In the Central Atlantic, the emplacement of the extensive Central Atlantic Magmatic Province (CAMP) in the early Jurassic is linked to thermal and tectonic processes preceding and during continental rifting (Nomade et al., 2007; Greenroyd et al., 2008; Buiter and Torsvik, 2014). As observed along other margins (e.g., Clemson et al., 1997; Gibson et al., 2013; Peace et al., 2018), reactivation of pre-existing structures likely focused the location of rifting (Attoh et al 2005; Mercier de Lépinay et al., 2016). Rifting was predominantly symmetrical within the Central Atlantic, involving normal faulting and the formation of rift basins (Withjack et al., 2012; Biari et al., 2017) until seafloor spreading commenced around 180–200 Ma (Labails et al., 2010; Mercier de Lépinay et al., 2016). While the CAMP coverage was extensive across West Africa and Northeast America (Marzoli et al., 2004), intercontinental deformation at this time was minor (Biari et al., 2017).

Along the Equatorial Atlantic are alternating zones of divergent and transform tectonics (Basile, 2015). Oblique transform rifting via an eastward propagating system of strike-slip faults initiated in the Early Cretaceous (ca. 140 Ma) forming fault bounded pull-apart basins (Ye et al., 2019). The Guinean Plateau, which sits at the transition between Central and Equatorial Atlantic systems, exhibits evidence of crustal thinning related to the initial Jurassic extension and deformation linked to later Cretaceous transform movement (Mercier de Lépinay et al., 2016). This suggests the Guinea-Liberia margin initially began rifting during Central Atlantic extension followed by the main transform rift phase during the Early Cretaceous (Bennett and Rusk, 2002; Ye et al., 2019).

Movement along E-W to ENE-WSW intra-continental transform faults continued through the Valanginian to Aptian (140–113 Ma) (Heine et al., 2013). The end of continental rifting of the Equatorial Atlantic is marked by a Late Albian Breakup Unconformity (107 – 100 Ma) mapped and correlated across diachronous oceanic crust from the Sierra Leone segment to the Togo-Benin segment of the margin (Ye et al., 2019). At the time of break-up, South American plate rotation shifted the tectonic regime of the Ivory Coast-Ghana margin segment from transtension to transpression (Attoh et al., 2004) and an angular breakup unconformity formed beneath Late Albian-Cenomanian Marine sediments (Fernie et al., 2018; Ye et al., 2019). The transition to seafloor spreading is marked by a so-called 'active-transform' stage from the Turonian to Santonian (ca. 94–84 Ma) as oceanic spreading continues along transform faults (Basile, et al., 2005; Nemcok et al., 2016; Ye et al., 2019; Fernie et al., 2018).

The tectonic processes that occurred during the formation of the West African Transform Margin has made this sector the type-example for this form of continental break-up (Basile,

2015). The margin exhibits a classic geometry with an outer corner, where the continental margin extends out towards the oceanic accretion axis, and inner corner, where the margin extends inwards towards the continent, created by the divergent margin segments being intersected and bound by major transform faults (Fig. 1a). There is also the presence of a transform fault parallel marginal ridge along the western side of the Romanche FZ where maximum strike-slip deformation has occurred (Fig. 1a, Basile, 2015) and transform marginal plateaus in the Guinean, Liberian and Côte d'Ivoire-Ghana offshore segments (Loncke et al., 2020).

2.2. Regional geology

The Guinea-Ivory Coast sector of West Africa is dominated by the Archean to Palaeoproterozoic granitoids and greenstones of the Leo-Man Shield (Fig. 1b). In Guinea, Archean gneisses in the west are separated from the younger Palaeoproterozoic rocks in the east by N-S and NE-SW trending shear zones (Rollinson, 2016; Traoré et al., 2022**).** The trend of these shear zones reflects the prevailing structural trend in western Ivory Coast, with basement structures accommodating transcurrent displacements during the Palaeoproterozoic orogeny (Lompo, 2010; Traoré et al., 2022). A more complex structural fabric is observed in southeast Guinea and western Sierra Leone where numerous faults crosscut one another and are the product of Pan-African deformation accommodating mostly strike-slip movements (Guiraud et al., 2005) (Fig. 1a,b).

Across West Africa, Pan-African basin inversion and thrusting is manifested as two distinct events (Villeneuve, 2005). The first Pan-African event occurred at ca. 660 Ma and formed the Mauritanides and Bassarides Belt, with the Mauritanides being reworked during Late Palaeozoic Hercynian deformation (Guiraud et al., 2005). The second event at ca. 550–500 Ma produced the NNW-SSE trending Rokelides Belt, which extends through southwestern Guinea, beneath the Bove Basin, and runs adjacent to the coastline through Sierra Leone and Liberia (Villeneuve and Cornée, 1994; Guiraud et al., 2005; Deynoux et al., 2006) (Fig. 1a).

The Neoproterozoic to Cambrian Madina-Kouta Basin, comprised of alternating continental and shallow marine sandstones, siltstones and shales, overlies the Leo-Man shield in northern Guinea and extends eastward through Mali and Burkina Faso along the southern margin of the larger Taoudeni Basin (Villeneuve, 2008; Ennih and Liégeois, 2008) (Fig. 1b). The Bové Basin in northern Guinea (Fig. 1a) sits on top of the pre-Cambrian basement and Pan-African belts and is comprised of Cambrian–Devonian shallow water platform sandstones and conglomerates, Silurian marine shales with interbedded sandstones, and alternating sequences of Devonian marine sandstones and shales (Villeneuve, 2005; Deynoux et al., 2006). Northwest of Guinea, in Guinea-Bissau, Upper Cretaceous sediments are present and belong to the larger Senegal Basin (Fig. 1a,b), which extends north along the Central Atlantic margin and west into the offshore domain (Brownfield and Charpentier, 2003). These rocks are primarily marine shales, siltstones and sandstones, which form the primary hydrocarbon reservoirs and seals in the Senegal Basin (Brownfield and Charpentier, 2003; Davison, 2005).

Emplacement of the CAMP (Fig. 1) is believed to have occurred during a short-lived (ca. < 1 Myr) period of peak magmatism at ca. 201 Ma followed by ongoing activity until ca. 192 Ma based on ^{40}-Ar/^{39}Ar and zircon ^{206}Pb/^{238}U ages (see Marzoli et al. 2018 for a review). Large volumes of mafic intrusive material were emplaced during this magmatism in the form of long, dense dyke swarms and voluminous sills (Deckart et al., 2005). Lava flows can be found and traced across sedimentary basins; however, they are thin (<500 m) and rarely preserved (Marzoli et al., 2018). Outcrop in Guinea is predominantly in the form of layered intrusions forming caps on elevated regions. Estimated pre-erosional volumes of the CAMP have been given in the range of 2–3x10^6 km^3 (McHone, 2003; Svensen et al. 2018) (Fig. 1b).

2.3. Topography and geomorphology

The topography in Guinea is dominated by the Guinea Rise topographic massif (Chardon et al., 2016) that trends NW-SE through Guinea, reaching elevations > 1000 m capped by low-relief plateaus (Fig. 2). Inward from the coast, a series of stepped escarpments mark rapid increases in elevation (up to 700 m) in northern Guinea. Across Sierra Leone and Liberia, a 100–200 km wide low-relief, coastal plain with a gentle elevation increase up to ca. 200 m is observed. Along the Guinea sector of the Central Atlantic margin, the coastal plain is narrower < 100 km, with a region of high relief and elevations up to ca. 600 m, following the structural trend of the Rokelide Belt, separating the coastal region from the Guinea Rise. Four hundred kilometres inland, the topography drops to a low-relief, gently inland sloping region with elevations of ca. 400 m (Fig. 2). In the southern part of the Guinea Rise, the elevated plateau is fragmented with the eastern crest of the plateau studded with a series of N-S trending ridges following the cratonic shear zone trends. Further south, the relief, comprised of peaks and scattered plateaus, is controlled by the NE trending structural grain of the basement with maximum elevations reaching 1948 m on Mont Loma in NE Sierra Leone. Maximum elevations across Ivory Coast are lower than along the Central Atlantic margin. Elevation gently increases from sea-level at the coast to ca. 400–600 m at 500 km inland.

The Guinean Rise is one of three major topographic features (including the Hoggar swell in the north and Jos Plateau to the east), that control the large-scale regional drainage of West Africa (Chardon et al., 2016). These features form part of the continental-scale basin-and-swell topography (Burke, 1996), which is proposed to be a product of long-term surface processes in response to the break-up of Gondwana, post-rift tectonics and intraplate mantle driven dynamic uplift (Burke, 1996; Chardon et al., 2016). The drainage is divided by Grimaud et al. (2018) into 4 main domains: (i) Senegambia (ii) Short Atlantic drainages, (iii) Long Atlantic drainages, and (iv) the Niger catchment (Fig. 2). The existing drainage network is suggested to have been relatively stable since the early Oligocene (29 Ma) or possibly earlier at the end of the Eocene (34 Ma) (Chardon et al., 2016).

Reconstruction of the Cenozoic drainage evolution has been achieved through a series of studies using ^{40}Ar-^{39}Ar dating of K-rich Mn oxides and regionally correlated remnant lateritic palaeo-landforms across West Africa (e.g., Vasconcelos et al., 1994; Beauvais et al., 2008; Beauvais and Chardon, 2013; Grimaud et al., 2014; Chardon et al., 2016). Several weathering sequences were identified and include the bauxitic "African Surface", which developed under humid conditions from the Late Cretaceous to ca. 45 Ma, the ferricrete capped "Intermediate" surface, which developed between 29 and 24 Ma, and three Neogene pediment systems abandoned at ca. 11, 6 and 3 Ma, respectively, known as the High, Middle and Low glacis systems (Beauvais and Chardon, 2013; Chardon et al., 2016, 2018; Grimaud et al., 2014, 2018). Dissection of these landforms have enabled facilitated estimates of dissection driven denudation to be made with rates being extremely low since the Eocene (ca. 2–10 m/Myr, mean values of 5–7 m/Myr) (Beauvais and Chardon, 2013; Grimaud et al., 2014, 2018).

2.4. Previous thermochronology studies.

The new AFT data we present here compliments and adds to existing thermochronology data across the West African Equatorial

margin (Fig. 1a). Gunnel (2003) presented central AFT ages from Burkina Faso, ranging from 175 ± 10 to 218 ± 7 Ma, and thermal histories implying slow monotonic cooling since the Mesozoic at the core of the West African craton. In Ghana, Lisker et al. (2008) and Fernie et al. (2018) present AFT data from samples along the coastline and continental interior, respectively. AFT ages from basement samples along the southern Ghanian coastline range from 130 to 415 Ma (Lisker et al., 2008). Thermal history modelling of this data infers two stages of cooling during the Palaeozoic, following the Pan-African Orogeny, and Cretaceous, related to exhumation following continental rifting. Inland, central AFT ages range from 65 ± 11 to 298 ± 18 Ma (Fernie et al., 2018) with thermal histories inferring Late Triassic - Early Jurassic cooling attributed to post-CAMP thermal relaxation, early to mid-Cretaceous cooling (145 – 90 Ma) due to rifting related exhumation, and Late Cretaceous-Cenozoic cooling due to exhumation driven by post-rift tectonic reactivation along the Bole-Nangodi shear zone (Fig. 1a). Further east, along the Benin sector of the margin Wildman et al. (2019) present AFT ages ranging from 106 ± 5 to 401 ± 45 Ma with single-grain apatite (U-Th)/He ages (corrected for alpha-ejection) ranging from 26 ± 4 to 500 ± 95. These data and associated thermal history modelling are used to advocate for relatively rapid exhumation driven cooling in the Early Cretaceous along the coastal margin and the interior Iullemmeden Basin (Fig. 1a) and slower and lower magnitude cooling of the region between the coast and the Iullemmeden Basin through the Palaeozoic to present. The thermochronometery study in Benin does not preclude heating related to burial along the coastal basins and interior basins during the mid-Cretaceous (110 – 90 Ma) and Late Cretaceous to Early Cenozoic, respectively.

Offshore, Clift et al. (1998) and Bigot-Cormier et al. (2005) present AFT data from sedimentary samples collected from Ocean Drilling Program borehole sites through and surface samples along the marginal ridge (Fig. 1a). Clift et al. (1998) present central AFT ages from the borehole sites ranging from 88 ± 4 Ma to 113 ± 4 Ma. Central ages for samples from the southern continental slope of the ridge, reported by Bigot-Cormier et al. (2005) have a comparable but slightly larger range from 64.2 ± 4.7 to 125.3 ± 10. 6 Ma, with the majority of AFT ages younger than 100 Ma. Thermal history modelling of the data presented by Clift et al. (1998) infers pre-depositional cooling, which represents evolution of the source region (i.e., the evolving continental margin), between 130 and 110 Ma in three samples and between 110 and 100 Ma in another. Minor post-depositional heating and fission-track annealing is inferred following deposition. Clift et al. (1998) suggest the first cooling event was driven by uplift and erosion during transform deformation and a later cooling event by a post-transform period of inversion, respectively. As the majority of the AFT ages presented by Bigot-Cromier et al. (2005) are younger than the samples of Lower Cretaceous stratigraphic ages, they advocate significant sedimentary burial of these samples followed by erosion during the 'active-transform' stage.

3. Apatite fission track thermochronology

3.1. AFT methods

Apatite fission-track ages were obtained from 24 samples from Guinea and 11 from the Ivory Coast using the zeta-calibration external detector method (Hurford and Green, 1983). Apatite fission-track ages were combined with horizontal confined track length measurements to constrain thermal annealing of tracks through the AFT partial annealing zone (PAZ, 60–110 ± 10 °C) (Gleadow et al., 1986). The angle of measured track lengths to the crystallographic c-axis was measured to correct for anisotropic annealing (Ketcham et al., 2007) and Dpar (length of the etch pit formed by tracks intersecting the polished grain surface) was measured as a proxy for the bulk compositional influence on track annealing (Carlson et al. 1999; Donelick et al. 2005). Radial plots and track length distributions for all samples can be found in Supplementary Data, Fig. S1 and Fig. S2, respectively.

3.2. Apatite Fission-Track results

3.2.1. Guinea

Twenty-four samples were collected from Guinea (Table 1; Supplementary Data, Table S1) and can be divided into two regional groups (Fig. 2). In the northwest, 15 samples (Guinea North) form a coast-perpendicular transect that extends from the coast, through the elevated Guinean Rise to ca. 400 km inland. Nine samples (Guinea South) cover the south-eastern region of the Guinean Rise at ca. 800–1000 m elevation. Central AFT ages across the entire Guinea dataset range from 99.1 ± 13.0 to 204.2 ± 34.3 Ma. Nine samples fail the $P(\chi^2)$ age homogeneity test (i.e., $P(\chi^2) < 0.05$) with four of these samples showing excess single grain age dispersion (>20%) than that expected for a single population (see radial plots in Supplementary Data, Fig. S1). In most of the Guinea samples, Dpar measurements were collected across the entire sample (i.e., not on individual dated grains) and so the relationship between single grain age and Dpar cannot be assessed. In those samples where Dpar was measured on dated grains (Supplementary Data, Fig. S1) no relationship between Dpar and age is apparent suggesting excess scatter cannot be solely attributed to apatite composition influence annealing. Given the high number of tracks for the samples in the Guinean dataset, it is possible that the chi-sq test is penalising the data for being too precise (e.g., Vermeesch, 2021). Mean track lengths (MTL), corrected for their c-axis orientation (c-MTL) range from 13.57 ± 0.12 to 14.78 ± 0.08 with standard deviations of 0.78 to 1.47.

The Ivory Coast dataset contains 11 samples (Fig. 2) (Table 1; Supplementary Data, Table S1) forms a broadly coast perpendicular transect from the coast to ca. 500 km inland with a gradual elevation gain from sea-level to 500 m. Approximately 350 km from the coast, two samples (YOR-1 and YAL-1) fall to the west of the main transect along an outer ridge of the Guinean rise. Central AFT ages in Ivory Coast range from 114.7 ± 13.1 to 188.9 ± 22.5 Ma, c-MTLs range from 13.99 ± 0.14 to 14.39 ± 0.07 μm with unimodal track length distributions and MTL-SD of 0.74–1.03. Five samples fail the $P(\chi^2)$, however, only one of these samples show excessive dispersion (>20%). As suggested above for the Guinean samples, apatite composition variability may have an influence on creating excess single grain age dispersion but the high track counts in these grains may be a contributing factor causing the $P(\chi^2)$ to fail.

Our West African data set yields a relatively narrow range in MTLs 13.57 ± 0.12 to 14.78 ± 0.08 over a reasonably large age range 99.1 ± 13.0 to 204.2 ± 34.3 Ma, which does not show any clear correlation (Fig. 3a). The negative correlation between MTL and MTL St. Dev. (Fig. 3b) reflects shorter MTLs having a broader track length distribution.

Inland from the coast, AFT ages in the Ivory Coast and the northern Guinea increase gradually to a distance of ca. 200 km (Fig. 3c). In northern Guinea, this distance corresponds to the region of increasing topography from sea-level at the coast to the highest sampled elevations in the Guinean Rise (i.e., samples GN-06 to GN-08) (Fig. 2). The relationship to topography is less clear in Ivory Coast due to the modest elevation range across the entire country (Fig. 2). However, in general this ca. 200 km region corresponds to the low-lying (<200 m) coastal strip.

Beyond 200 km inland, AFT ages gradually decrease again (Fig. 3c). This is best observed in the Guinea North dataset, with three samples from Ivory Coast also plotting on this trend. In

Table 1
Apatite Fission Track data. ρ_s, ρ_i, ρ_d are track density of induced, spontaneous, dosimeter tracks. P(χ2) is p-value of the chi-sq age homogeneity test (Galbraith, 2005). AFT ages are central ages calculated with 1σ standard error. 'GN' samples were etched using 5 M HNO3 after Gleadow and Lovering, (1978) and ages were calculated using a ζ = 338 ± 38 with a standard CN-5 glass. All other samples were etched using 5.5 M HNO3 after Donelick et al. (2005) and ages calculated with ζ = 303.1 ± 9.6 using a standard IRMM540 glass. Dispersion is the standard deviation of the single-grain ages as a percentage of their central age. Mean track lengths are corrected for their orientation to the c-axis after Ketcham et al. (2007). Sample location and rock type information are found in Supplementary Data, Table S1.

Sample	ρ_s	ρ_i	ρ_d	C. AFT Age	# Xtls	MTL	St. Dev.	proj. MTL	St. Dev.	# L	P (χ^2)	Disp.	D_{par} (µm)
	($x10^5 cm^{-2}$)			(Ma)		(µm)		(µm)					
Guinea North													
GM14-01	9.2	21.8	15.5	99.1 ± 13.0	18	12.71 ± 0.19	1.29	14.13 ± 0.13	0.87	45	0.00	27%	1.78 ± 0.18
GM14-02	18.4	39.0	15.3	109.8 ± 12.3	20	12.92 ± 0.08	1.21	14.28 ± 0.05	0.83	262	0.00	14%	1.89 ± 0.17
GM14-12	15.3	22.4	15.2	156.1 ± 17.4	20	13.59 ± 0.11	1.13	14.78 ± 0.08	0.78	101	0.11	8%	2.06 ± 0.15
GM14-13	6.5	11.9	15.0	126.6 ± 14.3	20	13.37 ± 0.11	1.11	14.60 ± 0.08	0.78	103	0.32	1%	1.79 ± 0.16
GM14-14	7.7	13.6	14.9	124.4 ± 15.4	20	13.12 ± 0.17	1.38	14.45 ± 0.12	0.94	64	0.00	23%	1.84 ± 0.14
GN-01	4.9	11.3	13.5	109.6 ± 16.2	25	12.46 ± 0.16	1.6	13.57 ± 0.12	1.25	101	0.89	0%	2.12 ± 0.24
GN-03	15.2	32.2	13.7	121.8 ± 17.7	25	12.80 ± 0.19	1.87	13.82 ± 0.14	1.41	95	0.80	0%	2.24 ± 0.25
GN-04	19.9	39.1	14.1	138.0 ± 21.8	24	12.75 ± 0.21	1.47	13.77 ± 0.17	1.19	47	0.00	29%	2.31 ± 0.26
GN-06	5.0	8.7	14.3	153.4 ± 23.3	40	13.45 ± 0.14	1.37	14.35 ± 0.10	1.03	100	0.36	14%	2.48 ± 0.24
GN-07	15.0	25.1	14.5	163.2 ± 25.9	5	13.31 ± 0.59	2.13	14.25 ± 0.41	1.47	13	0.18	3%	2.28 ± 0.37
GN-08	8.9	14.5	14.8	171.1 ± 25.7	30	13.19 ± 0.14	1.45	14.16 ± 0.11	1.10	100	0.80	0%	2.44 ± 0.21
GN-09	2.5	4.8	15.0	145.1 ± 22.6	21	13.58 ± 0.14	1.28	14.51 ± 0.10	0.93	85	0.54	3%	2.11 ± 0.23
GN-10	16.1	32.7	15.2	137.3 ± 4.1	20	12.89 ± 0.15	1.56	13.89 ± 0.12	1.20	102	0.12	6%	2.03 ± 0.20
GN-11	27.4	55.7	15.4	142.2 ± 20.6	15	12.83 ± 0.14	1.37	13.93 ± 0.10	1.00	102	0.51	1%	2.13 ± 0.25
GN-12	10.8	23.6	15.6	134.6 ± 19.7	20	12.23 ± 0.16	1.57	13.80 ± 0.09	0.93	100	0.20	6%	2.02 ± 0.20
Guinea South													
GN-13	25.5	47.8	15.8	156.2 ± 22.5	20	12.76 ± 0.14	1.40	14.04 ± 0.10	1.02	103	0.67	0%	2.32 ± 0.25
GN-16	18.4	42.7	16.1	129.9 ± 19.2	20	12.38 ± 0.16	1.58	13.81 ± 0.12	1.16	101	0.00	14%	2.26 ± 0.24
GN-18	12.8	19.1	16.3	204.2 ± 34.3	18	12.14 ± 0.18	1.81	13.73 ± 0.12	1.24	100	0.00	30%	2.18 ± 0.23
GN-19	26.8	50.4	16.5	164.3 ± 23.6	20	12.84 ± 0.14	1.42	14.04 ± 0.11	1.18	109	0.92	0%	2.31 ± 0.22
GN-31	13.4	27.8	14.3	129.9 ± 18.8	21	12.73 ± 0.15	1.46	13.84 ± 0.11	1.11	101	0.51	0%	2.14 ± 0.22
GN-33	8.3	17.8	14.6	127.0 ± 19.3	15	12.85 ± 0.16	1.55	13.85 ± 0.12	1.18	100	0.04	12%	2.13 ± 0.23
GN-34	13.2	26.1	14.8	140.3 ± 20.9	20	12.89 ± 0.14	1.42	13.84 ± 0.11	1.08	100	0.02	14%	2.34 ± 0.23
GN-36	20.3	37.9	15.0	150.5 ± 21.8	20	12.59 ± 0.14	1.41	13.69 ± 0.11	1.08	102	0.21	6%	2.26 ± 0.21
GN-37	21.0	43.0	15.2	139.1 ± 20.8	20	12.70 ± 0.12	1.25	13.80 ± 0.10	0.97	104	0.00	16%	2.14 ± 0.20
Ivory Coast													
DLO3bisA	31.7	50.1	15.8	149.9 ± 16.1	20	12.62 ± 0.13	1.56	14.07 ± 0.08	1.03	149	0.00	14%	1.88 ± 0.18
MK64	26.2	34.1	16.1	183.4 ± 20.6	20	12.63 ± 0.11	1.17	14.02 ± 0.08	0.83	116	0.00	14%	2.02 ± 0.16
SA-3	12.0	21.1	14.0	120.4 ± 13.6	22	12.58 ± 0.13	1.31	14.10 ± 0.09	0.89	113	0.00	13%	1.75 ± 0.19
YOR-1	11.4	21.3	13.7	117.6 ± 15.4	21	12.82 ± 0.14	1.45	14.27 ± 0.09	0.90	106	0.00	32%	1.81 ± 0.18
SEN-1	6.2	8.0	14.7	188.9 ± 22.5	20	12.93 ± 0.14	1.45	14.34 ± 0.09	0.92	100	0.04	15%	1.70 ± 0.14
YAL-1	16.9	23.0	14.4	159.3 ± 18.5	20	13.11 ± 0.11	1.13	14.39 ± 0.07	0.74	102	0.09	10%	1.77 ± 0.17
SOK-1a	7.5	11.1	14.3	144.6 ± 16.5	19	13.01 ± 0.19	1.31	13.99 ± 0.14	1.00	50	0.11	9%	1.72 ± 0.16
KG-33a	13.5	20.6	13.5	133.1 ± 14.6	20	13.03 ± 0.12	1.25	14.39 ± 0.07	0.76	103	0.14	6%	1.84 ± 0.17
SA-14	6.5	13.6	15.9	114.7 ± 13.1	20	13.15 ± 0.11	1.17	14.17 ± 0.08	0.83	100	0.25	7%	1.87 ± 0.15
VAA-1	9.4	15.1	13.4	124.3 ± 13.8	20	12.60 ± 0.14	1.39	14.11 ± 0.08	0.84	102	0.39	4%	1.68 ± 0.19
BEZ-1	9.4	15.0	14.1	132.2 ± 14.7	25	12.80 ± 0.14	1.4	14.19 ± 0.09	0.93	100	0.86	0%	1.65 ± 0.16

northern Guinea, the decreasing trend is coincident with a general decrease in elevation from peak elevation > 1000 m in the Guinean rise to ca. 400 m inland (Fig. 2). Although some of the Ivory Coast data agree with the lateral trend in AFT age, the elevation beyond 200 km inland gradually increases to ca. 400 m. Four samples from the Ivory Coast profile also appear to form a negative correlation from ca. 350 to 500 km inland that is offset from the main data trend (Fig. 3c). This type of offset may be attributable to fault offsetting with down-to-the-northeast displacement and differential denudation across the fault. However, more samples would be required to better relate the spatial relationship of the AFT data to fault displacement. Samples from the Guinea South dataset, situated between 300 and 400 km inland, are fairly scattered. Five samples appear to have AFT ages consistent with the main AFT age-distance from coast trend, while two seem more consistent with the offset trend defined by the Ivory Coast samples.

The Guinea North dataset shows the strongest AFT age-elevation correlation (Fig. 3d), which connects increasing and decreasing elevations across the Guinean Rise to the AFT age-distance from the coast relationship. The Guinea South data are more scattered but while they do not show a strong correlation, they appear to be consistent with the Guinea North AFT age-elevation trend. Several of the Ivory Coast samples fall on the trend defined by the Guinea North data but at 350–400 m there is more scatter in the Ivory Coast AFT ages. The offset samples here are also the samples that form the offset part of the AFT age-distance from the coast trend for Ivory Coast.

4. Thermal history modelling

4.1. Modelling approach

Thermal histories for all samples were acquired using QTQt, which incorporates a Bayesian transdimensional Markov Chain Monte Carlo (MCMC) approach to data inversion (Gallagher, 2012). Apatite fission-track data were modelled using the multi-kinetic fission-track annealing model of Ketcham et al. (2007) with anisotropic annealing and compositional influences on the annealing rate taken into account using c-axis projected track lengths and sample average Dpar measurements, respectively. We present the expected thermal history (ExTH) and 95% credible intervals in Fig. 4 and summarise the modelling results below. We provide a more detailed discussion of the modelling strategy, preliminary testing, alternative model scenarios and plots of the observed data vs. model predicted data in Supplementary Data, Data S1, Table S2, Fig. S3–S9. All QTQt input files are provided in Supplementary Data, Dataset S1.

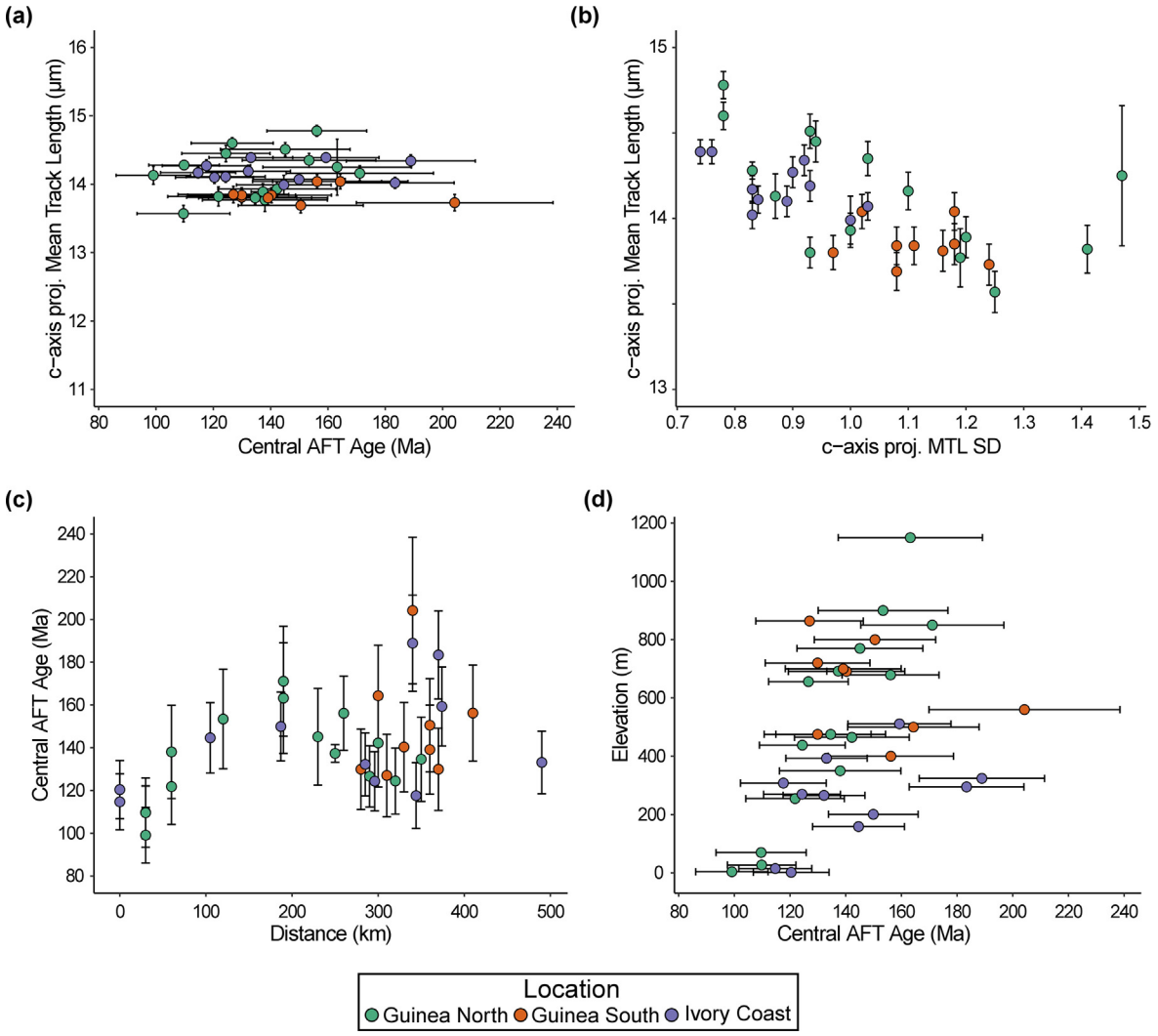

Fig. 3. AFT data plots: (a) c-axis projected mean track length vs. Central AFT age, (b) c-axis projected mean track length vs. c-axis projected mean track length standard deviation, (c) Central AFT age vs. Distance from the coastline, (d) Elevation vs. Central AFT Age. All uncertainties are 1σ.

Our modelling strategy involved initially modelling all samples individually and without any additional constraints to generate thermal histories with complexity solely driven by the data of one sample (Supplementary Data, Fig. S3). We then look to combine samples with the aim of reinforcing mutually consistent features observed in individual sample thermal histories and making these parts of the thermal history more robust. We take this step because due to the relatively low precision of AFT thermochronology, the data for a single sample may not robustly constrain detail in the thermal history the model (i.e., timing of maximum heating or inflection points in the thermal history path). Moreover, thermal histories from single samples taken from locations near to one another may result in apparent regional variability in thermal histories between adjacent samples. These variations in thermal histories could be interpreted as having a geological meaning (e.g., migrating patterns of erosion or fault movement causing differential denudation). Before this conclusion can be drawn, it should be assessed whether data from several samples within a region can be explained by a single thermal history that is consistent with all the data and their uncertainties. A multi-sample thermal history may also identify a sample or samples that are inconsistent with data from adjacent samples, and this may indicate a more complex spatial-thermal history relationship.

We take a simplistic approach to grouping samples, grouping first into 100 km bins (starting from the coastline), and assessing whether the joint model suitably reproduces all of the grouped data. If some samples are not reproduced, we group the data into 50 km bins, and then, if necessary to fit the data, resort to the individually modelled sample (see Supplementary Data, Data S1, Fig. S4 for further details). We assign a temperature offset based on an assumed geothermal gradient of 25 ± 5 °C/km. However, it should be appreciated that these samples do not form a pseudo-vertical profile or are not taken from a borehole profile where the definition of a thermal offset would have more relevance. The grouped samples are typically at similar elevations, have the same present-day surface temperatures and assumed to have had similar palaeo-temperatures. The specified geothermal gradient and the range on this value is used to build some uncertainty into this assumption.

We do not explicitly define an initial starting constraint for the models and in some cases the output thermal history appears to begin at temperatures somewhere much colder than the base of the PAZ. In these circumstances it is inferred that rapid cooling

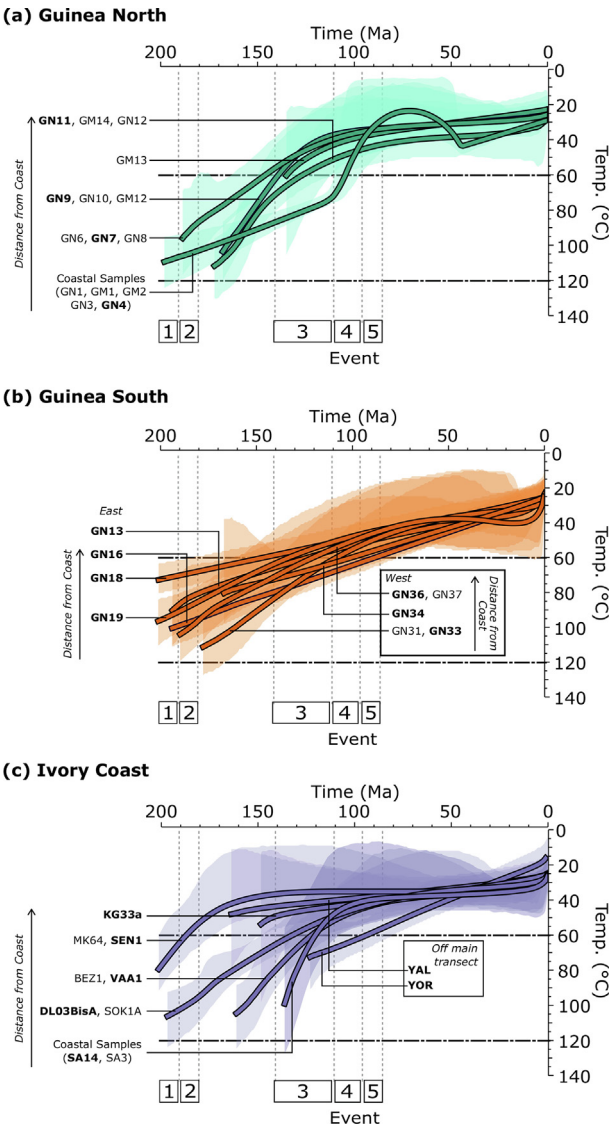

Fig. 4. Thermal history models for samples from (a) Guinea North (b) Guinea South, and (c) Guinea South. Thermal histories for each sample or sample grouping in each area are overlain on each other. Further details on the modelling methodology and sample groupings are provided in Supplementary Data, Data S1, Table S2, Fig. S3–S9. Thick line coloured line with black trim is the Expected Thermal History, coloured semi-transparent shading is the 95% credible intervals. Events correspond to 1: End of the CAMP activity, 2: Onset of sea floor spreading in the Central Atlantic, 3: Oblique transform faulting in the Equatorial Atlantic, 4: Continental break-up in the Equatorial Atlantic, 5: 'Active-transform' phase (Ye et al., 2019) in Equatorial Atlantic.

from temperatures hotter than the PAZ has occurred immediately before the starting point time.

4.2. Thermal history modelling results

4.2.1. Guinea North

Samples GM01, GM02, GN1, GN3 and GN4 reside on the low elevation coastal margin zone that extends 150–200 km inland from the coastline and are modelled together (Fig. 4a). The bauxite capped plateaus and pervasive Middle glacis relics in that area suggest that this part of the landscape experienced approximately 400 to 1000 m of denudation between 45 and 6 Ma, followed by negligible denudation to present-day. Assuming a geothermal gradient of 25 ± 5 °C/km from 45 Ma, and a surface temperature of 20 °C, this equates to cooling from a temperature in the range of 28 to 50 °C.

The geomorphological information can be used as additional constraints to force cooling from 45 and 6 Ma To prevent additional time–temperature points being proposed after 45 Ma, the lower time range of the prior was reduced to 45 Ma. The early portion of the ExTH (>70 Ma) shows the main cooling episode observed at ca. 110 Ma. Heating of ca. 20 °C is then inferred between 70 and 45 Ma, before finally cooling to surface temperatures at present-day as constrained by the geomorphology (Fig. 4b). In supplementary information (Supplementary Data, Fig. S5) we explore the necessity for the Early Cenozoic cooling event by forbidding reheating and observe that the data can still be reproduced without reheating. However, as this is a very restrictive constraint to impose, and the inferred reheating is fairly minor we continue our discussion with model presented in Fig. 4a.

While some ambiguity remains in the ExTH model, we can have confidence in the consistent and recurrent parts of the history. Specifically, this includes an initial period of protracted cooling through the Late Jurassic and Early Cretaceous followed by a phase of rapid cooling in the mid-Cretaceous (110 – 90 Ma). Some burial in the Late Cretaceous to Early Cenozoic prior to the samples cooling to the surface through the Late Cenozoic is possible, but not unequivocally required by the observed data. Regardless of the complexity of the Cretaceous and Early Cenozoic history, the samples remained at temperatures < 50 °C since the mid-Late Cretaceous (ca. 90 Ma).

The thermal history for samples *GN6, GN7* and *GN8* shows cooling from 100 °C at 190 Ma to 35 °C at 100 Ma. From 100 Ma to present the expected model predicts around 10 °C of cooling to surface temperatures, which is consistent with the low levels of denudation throughout the Cenozoic predicted by geomorphological studies (Beauvais and Chardon, 2013; Grimaud et al., 2018).

The GN09, GN10, GM12 thermal history reproduces the data well and shows cooling at a moderate rate between 100 and 40 °C from 170 Ma to 120 Ma before low levels of cooling from 120 Ma to present-day. The *GM13* single sample (Fig. 4a) also shows low amounts of cooling through low temperatures (i.e., <40 °C) from ca. 120 Ma but has experienced more rapid cooling at ca. 140 Ma.

Furthest from the coast, *GM14, GN11* and *GN12* yield a model where the top sample in the profile cools from 100 °C at 170 Ma to 60 °C at 135 Ma (Fig. 4a). The ExTH then predicts protracted cooling to bring the samples to present-day surface temperatures. The ExTH reproduces the data reasonably well and the path is consistent with the geomorphological constraints in the region.

4.2.2. Guinea South

All models across the Guinea South dataset (Fig. 2) show a similarly protracted cooling history (Fig. 4b). All samples cool through the base of the AFT PAZ during the Late Triassic to Late Jurassic, with the exception of *GN18*, which cooled through this boundary during the mid-Permian. Although slow cooling is predominant, there is some variation in the cooling rate through the Cretaceous (ca. 150–70 Ma) with some samples showing slower cooling and cooling through lower temperatures than others. For example, *GN18* experiences cooling from 61 to 42 °C at a rate of 0.24 °C/Myr between 150 and 100 Ma, compared to the joint model of *GN31* and *GN33* cooling from 90 to 42 °C at a rate of 0.6 °C/Myr.

4.2.2.1. Ivory Coast. Two samples, *SA14* and *SA3*, were collected from the coastline and when modelled together produce an ExTH that shows rapid cooling in the Early Cretaceous between 140 and 110 Ma (Fig. 4c), followed by minimal cooling until present day. The wide 95% credible intervals in the late Cretaceous imply that the initial cooling may have been greater than the expected

model shows, but it is also possible that these samples experienced some minor burial related reheating (<60 °C). The *DL03BisA* and *SOK1A* ExTH model shows cooling through the base of the PAZ at ca. 200 Ma, followed by a moderate cooling rate of ca. 0.6–0.7 °C/Myr through the Late Jurassic and Early Cretaceous, before the cooling rate drops quickly over the last 110 Ma (Fig. 4c).

Further inland, *BEZ-VAA* yields an ExTH model showing relatively moderate cooling through the PAZ during the Cretaceous with only minor, slow cooling through the Cenozoic (Fig. 4c). The *MK64-SEN* ExTH model shows cooling through the PAZ during the Late Triassic and Jurassic (ca. 215–150 Ma), and residence at near surface temperatures from the Cretaceous to the present-day (Fig. 4c). The ExTH model for the furthest sample from the coast, KG33, shows rapid cooling between 150 and 140 Ma followed by low-temperature (<40 °C) protracted cooling from the Cretaceous to present-day.

Two samples (*YAL* and *YOR*) sit west of the main transect (Fig. 2) on the Archean basement. *YOR* resided at the foot of an escarpment, which marks a jump in elevation from ca. 300 m to up to 1000 m. *YAL* is sampled inland of these maximum elevations, ca. 30 km northwest of *YOR*, from an elevation of 511 m. The individual models for these samples show an initially rapid phase of cooling at two distinct times. For *YAL*, cooling through the PAZ is inferred to occur between 170 and 155 Ma, while *YOR* infers rapid cooling from temperatures hotter from the base of the PAZ to ca. 70 °C at 120 Ma (Fig. 4c). As these samples are collected from a faulted region marking the boundary between the Archean basement and the reworked Archean and Proterozoic basement (Fig. 1), fault reactivation may have caused the distinct thermal histories.

5. Discussion

5.1. Spatial patterns of palaeo-temperature and denudation

Using the ExTH for the models presented above, we can infer the palaeotemperature pattern across the West Africa margin during specific time periods (Fig. 5). Assuming a geothermal gradient over time then allows us to estimate the amount of denudation or burial that may have occurred over time (Fig. 6). In Fig. 6 we highlight our denudation/burial estimates assuming a standard geotherm of 25 °C/km and use values derived from this geotherm in our discussion. However, we acknowledge that the geothermal gradient was likely elevated during continental breakup along passive and transform margins (Balázs et al., 2022) and the time of CAMP emplacement. We also acknowledge that the geothermal gradient more generally can vary over time and space due to deep thermal processes and due to the addition and removal of material with different thermal properties (e.g., Łuszczak et al., 2017) with implications for the temporal and spatial pattern of denudation. To reflect this, in Fig. 6 we show a range for denudation/burial estimates for geothermal gradients between 20 and 70 °C/km. The main observation that can be made using this range of values is that if geothermal gradients were higher and decayed over time, the total amount of material removed in the late Jurassic – Cretaceous would have been significantly less that that predicted using a gradient of 25 °C/km. However, it is not clear how far an elevated geotherm would have reached in the context of our sample locations relative to the main rift zone, and how this would have evolved in tandem with post-rift surface, tectonic and thermal processes. Acquiring thermochronometric data from different depths from borehole profiles would potentially yield greater insights into the evolution of the geotherm.

At 200 Ma, *MK64* and *SEN* reside at temperatures cooler that 120 °C (Fig. 5). All other samples were either residing at temperatures hotter than 100–120 °C at 200 Ma or were brought to temperatures hotter than 120 °C after 200 Ma but prior to cooling through the PAZ during the Cretaceous (Fig. 5). If these palaeotemperatures were solely due to burial, then this would equate to a total of 4 to 5 km of overburden that has been removed since the late Jurassic (for a geothermal gradient of (25 °C/km)). Most samples show a progressive decrease in the amount of cooling and consequently in denudation from the Early Cretaceous to the Cenozoic (Fig. 6). Some samples show slight increases in cooling in the Late Cenozoic, however, due to the low temperature nature of this cooling, it is uncertain.

The emplacement of CAMP rocks may have caused the temperature of upper crustal rocks to increase by direct heating due to their proximity to intrusions, associated regional hydrothermal activity, or burial of under thick layers of extrusive rocks, and/or changes in the geothermal gradient during magmatism and changes in thermal conductivity of the rock blanketing (i.e., the extrusive volcanic rocks) the previously exposed basement. CAMP lavas would have covered the 'pre-rift' landscape, which likely had some Palaeozoic cover (Hubbard, 1983). Given the location of the Guinean samples within the CAMP it is possible that this event reset the AFT data at ca. 200 Ma.

With the exception of samples *YAL* and *YOR,* the Ivory Coast samples lie out with the preserved CAMP intrusion field (Fig. 1b). If these samples were reset at ca. 200 Ma with the Guinean samples, then it is likely it was due to burial under CAMP extrusive rocks or more regional hydrothermal activity at the time. *MK64* and *SEN* have not been completely reset at this time, which may be due to their residence at a higher elevation and consequently not being covered by as thick a cover of volcanic rocks or less thick cover of Palaeozoic sediments. However, as the AFT data do not record when the data were reset, only when they cooled below the closure temperature, burial of the samples entirely beneath a sedimentary cover during the Palaeozoic cannot be excluded as a possibility.

For both transects, the samples nearest to the coast reside at the highest temperatures at 150 Ma (Ivory Coast samples are hotter than the base of the PAZ) and show episodes of rapid cooling (Fig. 5). In Guinea North, this rapid cooling occurs during the 110–90 Ma interval, after an initially moderate phase of cooling, whereas in Ivory Coast rapid cooling occurs during 130–110 Ma. Both of these events involve cooling of ca. 30–40 °C at a rate of 1.5–2 °C/Myr. For a geothermal gradient of 25 °C/km, this cooling equates to a denudation thickness of 1.2–1.6 km (Fig. 6) at a rate of 60 to 80 m/Myr.

In Guinea North, the interior samples cool at a low to moderate rate through the Early to mid-Cretaceous (~0.5 – 0.6 °C/Myr over 150–90 Ma) before the cooling rate and the total amount of cooling rapidly decreases through the Late Cretaceous and into the Cenozoic (~0.1 – 0.2 °C/Myr over 70–0 Ma). Similar trends in cooling rate and total amount of cooling through the Cretaceous and the Cenozoic are also observed along the interior of the Ivory Coast transect. Some of the initial cooling in the Early Cretaceous may be attributable to thermal relaxation following the CAMP event but it is also possible that a significant proportion of the cooling through the Early to mid-Cretaceous is attributable to exhumation driven by moderate erosion rates in response to continental breakup. This style of denudation pattern is comparable to that observed along passive continental margins worldwide (e.g., Gallagher and Brown, 1999; Persano et al., 2002; Spotila et al., 2004; Balestrieri et al., 2005; Campanile et al., 2008; Peulvast et al., 2008).

Due to the temperature sensitivity of the AFT thermochronometer, we are not able to resolve any detail on thermal events colder than 60 °C. However, our data remain informative as they require denudation to be less than ca. 1–2 km (Fig. 6). In the absence of data or any additional information driving inflections (e.g., epi-

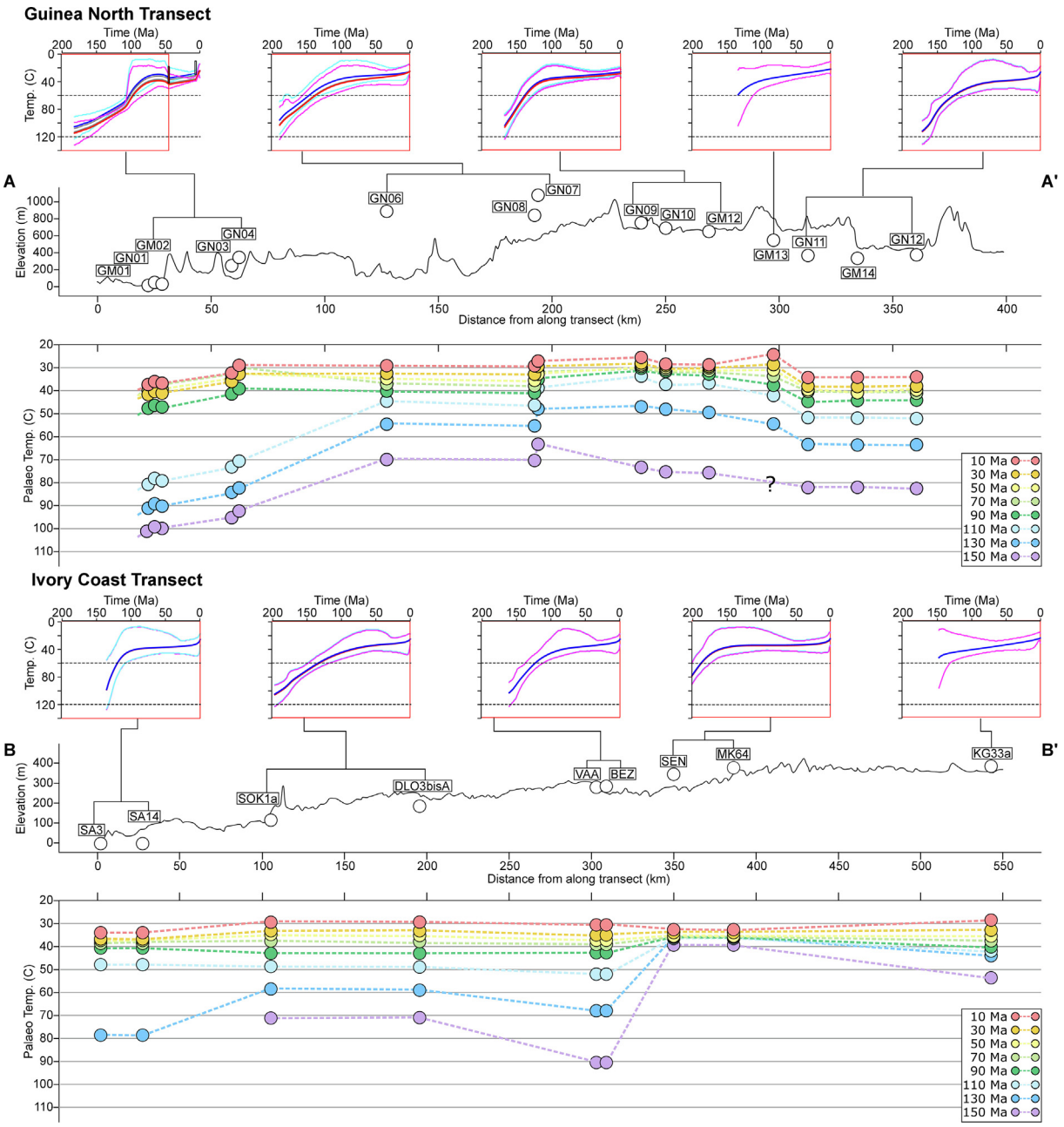

Fig. 5. Topographic profiles for the Guinea North and Ivory Coast transects with sample palaeotemperature at different time periods estimated from the expected thermal history model. Lines of transect are shown on Fig. 2. For clarity, palaeotemperature uncertainties are not shown but can be estimated using the 95% credible intervals on the expected thermal history.

sodes of rapid cooling or reheating) in the low-temperature thermal history during the Cenozoic our models infer simple monotonic cooling Our data and models are therefore consistent with observations by Beauvais and Chardon (2013) and Grimaud et al. (2014, 2018) that denudation was limited to ca. 2–10 m/Myr across this part of West Africa. Application of a lower temperature thermochronometer such as apatite (U-Th)/He would potentially provide additional insights on the timing and rate of Cenozoic cooling.

5.2. Thermal and tectonic processes along the West African margin.

Our new AFT data is an important contribution to a growing thermochronological record with coverage from the Guinean margin at along the Central Atlantic to the Benin margin along the Equatorial Atlantic (Fig. 7, Fig. 8). This regional dataset helps to better understand the spatial and temporal record of exhumation and the driving geological processes. All data from the West African transform margin are presented in an AFT age-MTL plot (Fig. 7a) and show a partial 'boomerang'-style relationship. 'Boomerang' relationships in AFT datasets are formed by a population of 'young' AFT ages and one of 'old' AFT ages, both with long MTLs, and a zone between these age populations where the AFT-MTL relationship follows a U-shaped trend. The data can be interpreted as preserving an early (old) rapid cooling event and then recording a later (young) rapid cooling event, with intervening samples exhibiting the effects of partial resetting (Green, 1986). In the West African data set the younger peak is evident corresponding to long MTLs (>12.5 μm) with Late Jurassic and Early- to mid-Cretaceous

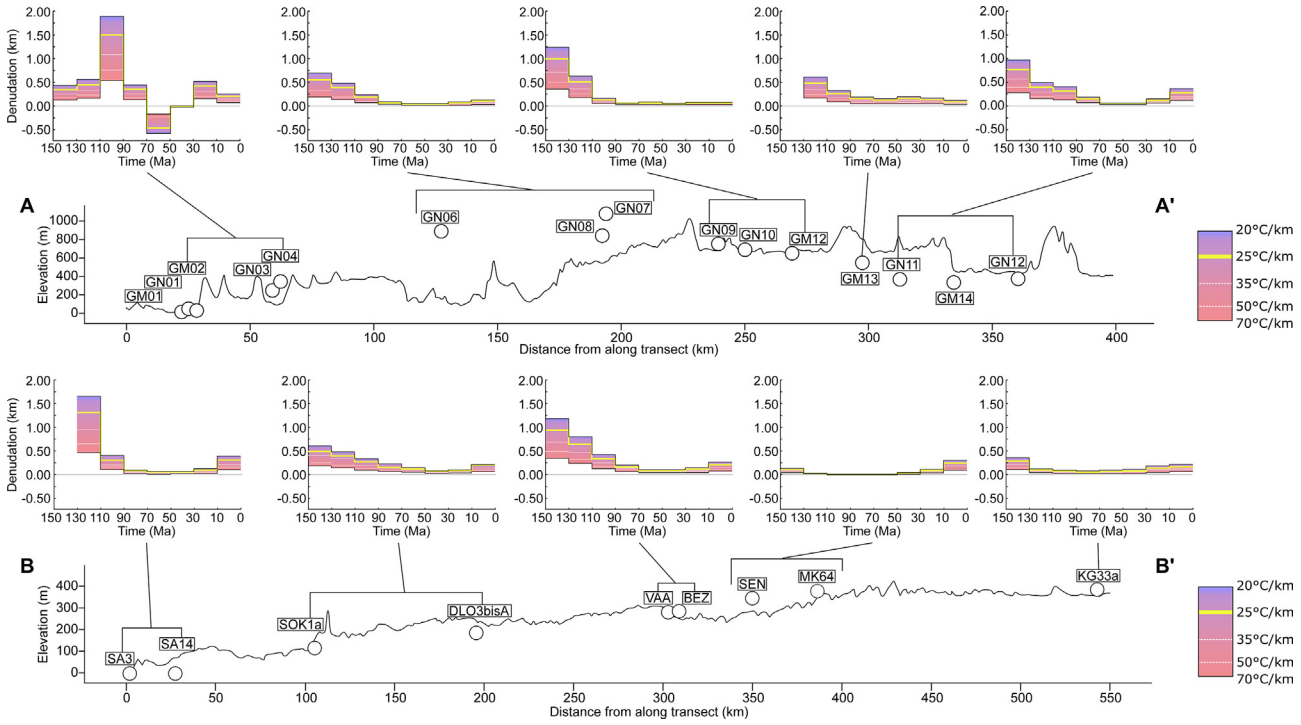

Fig. 6. Topographic profiles for the Guinea North and Ivory Coast transects with estimates of denudation for time intervals: 150 – 130, 130 – 110, 110 – 90, 90 – 70, 70 – 50, 50 – 30, 30 – 10 and 10 – 0 Ma. Yellow line highlights the estimates when a geothermal gradient of 25 °C/km is used. Bars show the range of possible denudation magnitudes for geothermal gradients between 20 and 70 °C/km. Lines of transect are shown on Fig. 2. (For interpretation of the references to colour in this figure legend, the reader is referred to the web version of this article.)

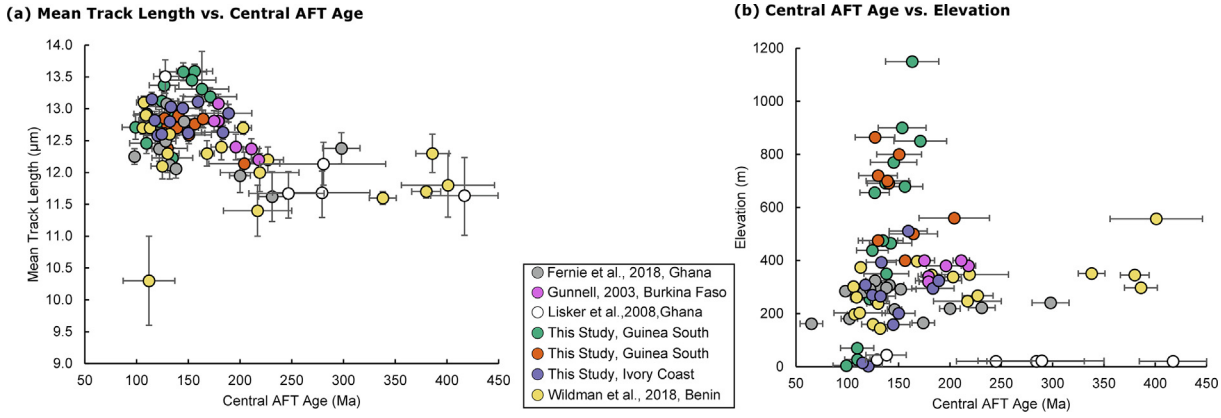

Fig. 7. West African AFT data plots: (a) Mean track length vs. Central AFT age. Measured mean track lengths (i.e., not c-axis projected lengths) are used because c-axis lengths are not presented in all publications) and (b) elevation vs. Central AFT age. All uncertainties are 1σ.

(145 – 90 Ma) AFT ages, signifying the importance of this period for the exhumation and cooling of West Africa, however, the older peak is absent. This suggests that all samples across this region of West Africa experienced some thermal annealing after the Cambrian/Early Ordovician.

The data defining the 'younger' peak are scattered due to variation in the AFT ages and MTLs. The long period of time over which samples yield long MTLs (Fig. 7a) may be indicative of temporal variations for the onset of cooling and variations in cooling rate across West Africa in the Mesozoic. The variation of the MTLs may be directly related to cooling, but it should be noted that Fig. 7a presents lengths that have not been corrected for their orientation to the crystallographic c-axis (e.g., Ketcham et al., 2007), which may improve consistency in the length measurements (Ketcham et al., 2018). Gunnell (2003), Clift et al. (1998), Bigot-Cormier (2005) and Fernie et al. (2018) do not state that a c-axis correction was made to the length measurements. The absence of this additional data is common in older studies as annealing anisotropy and appropriate numerical corrections were not typically considered. Some studies (e.g., de Grave et al., 2011; van Ranst et al., 2020) question the extent of anisotropy in fossil fission tracks and whether it is appropriate to make a c-axis correction, and this consideration may have been adopted by Fernie et al. (2018). Clift et al. (1998) and Bigot-Cormier et al. (2005) also do not include compositional information (e.g., Dpar or Cl wt. %), which is now commonplace in AFT studies. The absence of these data may help

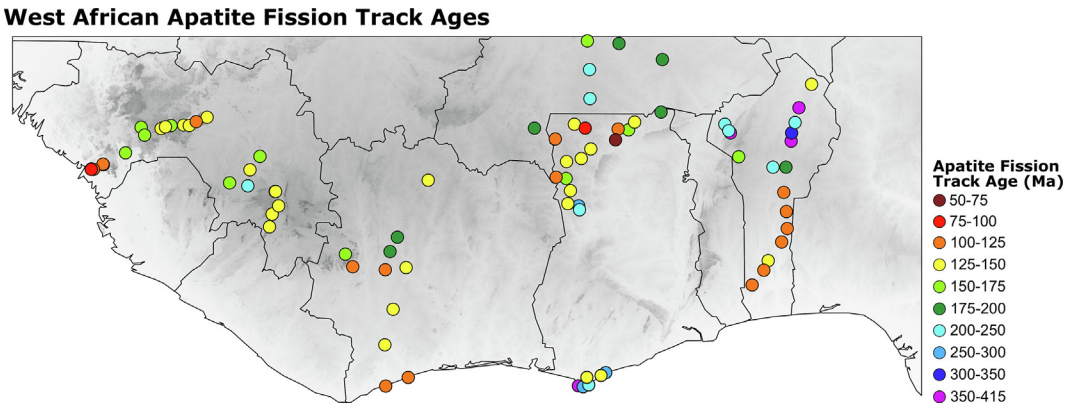

Fig. 8. Maps of West African published AFT data coloured to indicate AFT age. Sample source shown on Fig. 1a.

to explain some of the conflicts in timing in the thermal histories observed along the offshore marginal ridge by Clift et al. (1998) and Bigot-Cormier et al. (2005).

An AFT age-elevation relationship is most apparent in the Guinean samples, where a clear positive correlation is observed with increasing AFT age over ca. 1200 m of elevation gain (Fig. 7b). Despite AFT ages reaching up to ca. 400 Ma in Benin, no age-elevation relationship is apparent, with samples residing in a fairly narrow range of elevations ca. 200–400 m., suggesting prevailing lateral variations in erosion. It is also apparent that AFT ages>200 Ma (i.e., CAMP emplacement) are only found in datasets in the eastern part of the West African margin (e.g., Benin and Ghana). This lends further support to the thermal influence of the CAMP on the Guinean and Ivory Coast datasets and subsequent cooling driven by progressive exhumation of the Guinea and Ivory Coast regions of the West African margin (Fig. 9a,b).

The absence of the CAMP influence on the eastern datasets has made it possible to better observe the spatial variation in response of surface processes to major tectonic processes (Fig. 9). The lack of CAMP influence is inferred due to the preservation of relatively older (i.e., pre-CAMP) AFT ages in Benin (Wildman et al., 2019), Burkina Faso (Gunnell, 2003) and Ghana (Lisker et al., 2008; Fernie et al., 2018) (Fig. 1; Fig. 8). Samples with older (>200 Ma) AFT ages and relatively short MTLs in these studies reflect intracratonic regions that have experienced protracted cooling and slow rates and/or low magnitudes of erosion throughout the Palaeozoic and Mesozoic. However, Fernie et al. (2018) do present thermal histories that cool through the PAZ between 200 and 150 Ma, which they attribute to post-CAMP thermal relaxation.

Along the coastal strip in Benin, AFT ages are in the range 110 to 130 Ma. The jump to ages>300 Ma further inland, coincident with the location of the present-day continental drainage-divide at ca. 375 km (Fig. 8), is comparable to models of passive margin landscape evolution, where erosion during escarpment retreat or plateau downwearing drives exhumation (Wildman et al., 2019). Due to the flexural isostatic response to erosion, denudation magnitudes can be several kilometres and are greatest in the region between the coast and the continental divide (Fig. 9) (Gallagher and Brown, 1999; Braun, 2018; Wildman et al., 2019). While the increase in AFT age is not as dramatic along the Guinean and Ivory Coast margins a similar scenario may be invoked. Along the Guinea North transect, the trend of increasing AFT age with distance from the coast, and with increasing elevation, may also mark the influence of a drainage divide at ca. 200 km inland, where the oldest AFT ages are observed. In Ivory Coast, AFT ages progressively increase from the coast to ca. 350 km inland, where *MK64* and *SEN-1* preserve older AFT ages.

The patterns of long wavelength deformation, driving the exhumation patterns across the Central and Equatorial Atlantic, are consistent with the model of transform margin evolution described by Ye et al. (2017) involving the formation and persistence of flexural margin up-warps (e.g., Gilchrist and Summerfield, 1990; Gallagher and Brown, 1997) (Fig. 9). Within this model, the divergent Central Atlantic further North than our study area exhibits a longer wavelength, coast parallel, up-warp compared to the transform Equatorial Atlantic. The difference in up-warp wavelength is attributed to the age of the respective margins, with wavelength increasing for the older central Atlantic margin due to greater thermal relaxation and lithospheric strengthening (Ye et al., 2017). The main pattern of denudation following rifting in the Equatorial Atlantic extends ca. 350 km inland from the coast from Guinea along to Benin. However, in Guinea we have no data > 350 km from the coast along the Guinea North transect.

Across Guinea, Ivory Coast and Benin, samples inland of the divide infer Mesozoic cooling suggesting erosion of interior flanks of the marginal up-warp beyond the drainage divide (Fig. 9) that may have fed sediment into interior basins (see Ye et al., 2017). Ye et al. (2017) attribute the long wavelength of the Ivory Coast upwarp to processes in the asthenosphere and highlight the emplacement timing (150 and 135 Ma) of Leo-Man shield kimberlitic province in support for chemical and physical changes in the lithospheric mantle, which drives vertical motions (e.g., Ault et al., 2013; Stanley et al, 2015). However, the inference from our thermal histories that crustal cooling across the Ivory Coast was already underway in the late Jurassic-Early Cretaceous suggests a closer link to the tectonic and or thermal processes forming the up-warp along the divergent Guinean margin.

Thermal histories from samples from the coastline along Guinea North and Ivory Coast also support more rapid cooling events (Fig. 4a, Fig. 4c). These rapid cooling events may be attributed to more rapid exhumation due to erosion of short-wavelength uplift rift flanks. Along the Ivory Coast equatorial margin, the timing of this rapid exhumation is coeval with the main phase of transform faulting in the Equatorial Atlantic suggesting a causal link (Fig. 9c). Data from Benin (Wildman et al., 2019) and Ghana (Fernie et al., 2018; Lisker et al. 2008) suggest cooling driven by exhumation related to rifting and associated processes occurred along the entire Equatorial Atlantic margin and further into the continental interior (e.g., Benue Trough in Ghana, Gao rift in Benin). The abrupt transition in AFT ages in Ghana across the Bole-Nangodi shear zone (Fig. 1a, Fig. 8) invoke intracontinental reactivation, during the rift period, causing differential exhumation across the structure (Fig. 9) (Fernie et al. 2018). Possibly fault reactivation or hydrothermal cir-

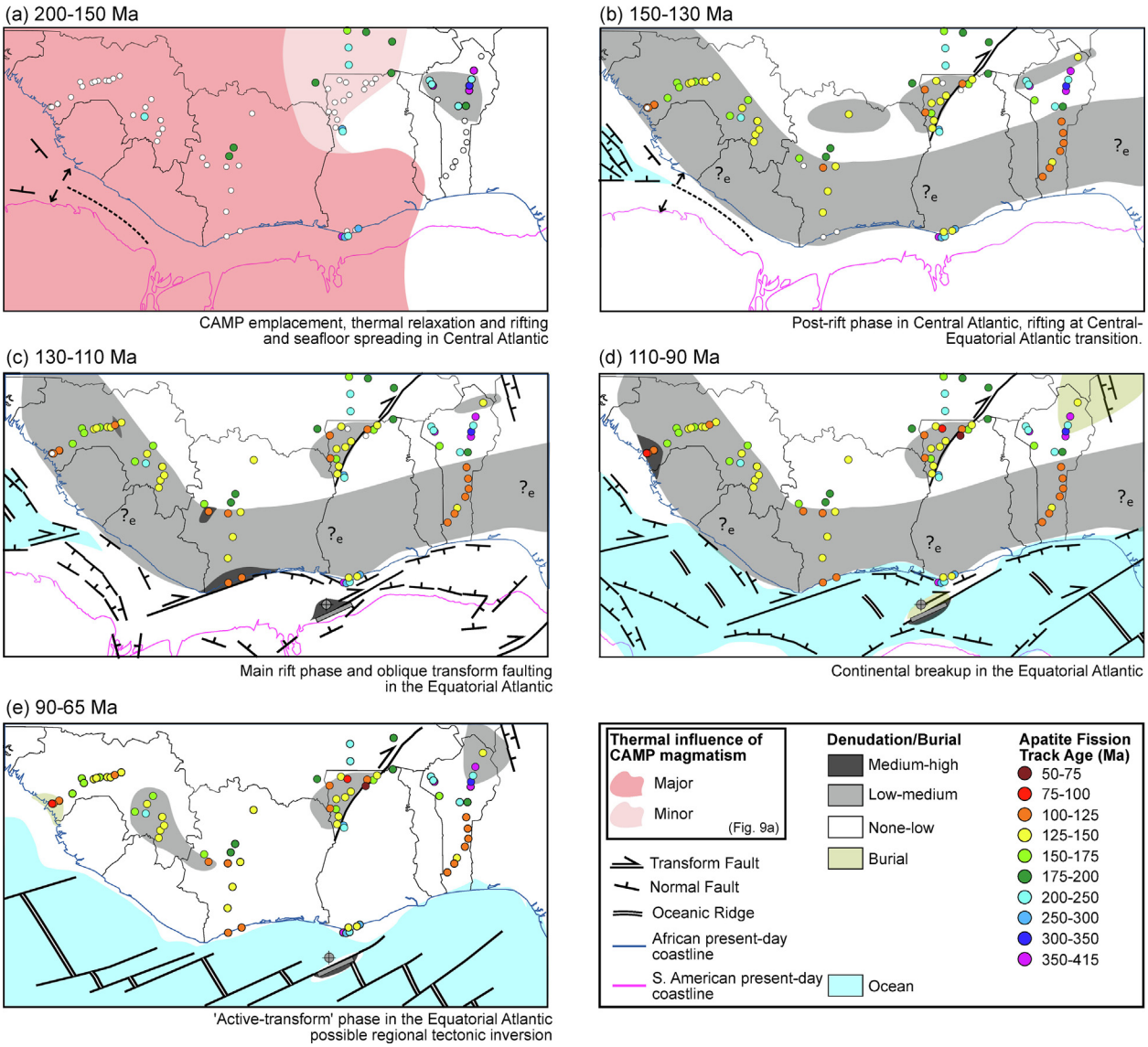

Fig. 9. Maps of West Africa summarising tectonic, thermal, and surface evolution over the Late Jurassic and Cretaceous. Palaeogeography and tectonics structures adopted after Ye et al. (2017). (a) During Late Jurassic the emplacement of the Central Atlantic Magmatic Province caused thermal resetting of samples across Guinea, Ivory Coast and potentially in Ghana. Samples in Benin are not reset and preserve a record of Palaeozoic denudation. (b) Denudation across the length of continental margin in response to rifting in the Equatorial Atlantic. Denudation inland due to erosion of marginal upwarps, inland of drainage divides or erosion of uplifted blocks due to intraplate fault reactivation along the Bole-Nangodi Shear Zone (Fernie et al., 2018). (c) Denudation along coastal margin and across some inland regions continues through late Early Cretaceous at moderate rates, faster denudation observed along the Ivory Coast coastline and the offshore marginal ridge in response to the main phase of rifting and onset of transform faulting in the Equatorial Atlantic. (d) Denudation is generally lower along continental margin during the mid-Cretaceous but enhanced denudation inferred along the Guinean coastline and the southward slope of the offshore Ivory Coast marginal ridge (Bigot-Cromier et al., 2005). Burial inferred inland in Benin along the margins of the Iullemmenden Basin (Wildman et al., 2019) and possibly the northern slopes of the offshore marginal ridge (Clift et al., 1998). (e) Denudation magnitudes are inferred to be low from the Late Cretaceous until present-day. Some interior regions continue to have low-moderate rates of denudation and another phase of intracontinental fault inversion may have occurred.

culation can explain the offset ages along the Ghanian coast (Fig. 8) (Lisker et al., 2008).

The rapid exhumation along the Guinea coastline is approximately 80 Ma after the onset of seafloor spreading in the Central Atlantic and overlaps with the end of transform faulting in the Equatorial Atlantic (Fig. 9d), possibly suggesting some regional tectonic uplift in response to continental break-up in the Equatorial Atlantic. Fernie et al. (2018) present central AFT ages as young as 65 ± 11 Ma and tentatively propose a Late-Cretaceous – early Cenozoic, minor cooling event, attributed to inversion during NNW-SSE shortening within western Africa driving a phase of enhanced exhumation. This timing would also be consistent with the timing of exhumation of the offshore marginal ridge proposed by Bigot-Cormier et al. (2005) (Fig. 9d,e). Reactivation of brittle faults during the syn- and post-rift phase has also been proposed along several type-example passive continental margins (e.g., Ksienzyk et al., 2014; Cogné et al., 2011; Wildman et al., 2016). Moreover, inversion during the Late Albian has been observed in structures along the Guinea plateau (Ye et al., 2017) and so fault reactivation along the Guinean coast, driving the rapid cooling between 110 and 90 Ma cannot be ruled out. Uplift and tectonic reactivation across the Central and Equatorial margins following continental break-up in the Equatorial Atlantic and through the active-transform phase is therefore possible but still poorly resolved by the AFT datasets.

The limitations on the temperature sensitivity of AFT thermochronology and the low magnitude of Mesozoic cooling make

resolving the thermal history and the chronology of denudation and burial through the Cenozoic challenging. Along the coastal regions of the Central and Equatorial Atlantic there are remnants of Late Cretaceous sedimentary basins (i.e., embayments). However, the past extent of these basins, in terms of both their regional coverage and thickness, is uncertain. Our data from Guinea and Ivory Coast and that presented by Wildman et al., (2019) from Benin do not exclude burial of the coast (e.g., Fig. 9e) and along the fringes of interior basins (e.g., Fig. 9d) as a possibility but they do infer that any burial was not sufficient to cause significant track annealing and so the total amount of heating related to this burial was < 60 °C.

More generally across West Africa, the chronology of landscape evolution has been resolved using dated relict lateritic landforms (Beauvais and Chardon, 2013; Grimaud et al., 2014; Chardon et al., 2016). These datasets all appear to converge on the conclusion that in West Africa there was greater tectonic stability and lower magnitudes of erosion during the Cenozoic and certainly since the Eocene. Surface uplift during the Cenozoic, driven by mantle upwellings, has been proposed as a mechanism to form the 'basin-and-swell' topography described across Africa (e.g., Burke, 1996). The growth of the Hoggar Swell, to the northeast of our study area, since the mid-Eocene caused significant denudation and increase in sediment flux from the Niger-Benue catchment (Chardon et al., 2016; Grimaud et al., 2018). Elsewhere in West Africa any minor surface uplift contribution of mantle driven upwelling did not trigger km-scale erosion (Grimaud et al., 2018). Instead, erosion would have been limited to enhanced dissection of successive weathering profiles.

The regional drainage network response to tectonic and isostatically driven surface deformation will determine how the eroded sediments are partitioned into offshore and interior basins (e.g., Ye et al., 2017). A source-to-sink analysis by Ye (2016) observe that in the Ivory Coast–Ghana basin the largest accumulation of siliciclastic sediments occurs during the Campanian (85–72 Ma). Over the mid-Late Cretaceous (104 – 66 Ma), accumulation rates increase from 4.3 to 13.3 $\times$ 10^3 km^3/Myr. At this time, most samples across the Guinea and Ivory Coast margins, except for the coastal samples in Guinea, show very low cooling rates, or rapidly decreasing cooling rates, reflecting slow, low-magnitude exhumation. These low cooling rates continue throughout the Cenozoic, while offshore accumulation rates first decrease in the Eocene to 3.3 $\times$ 10^3 km^3/Myr before increasing to 12.3 $\times$ 10^3 km^3/Myr in the Plio-Pleistocene, with a short-lived peak of 18.3 $\times$ 10^3 km^3/Myr in the Early Oligocene (34–31 Ma). The general trend observed in the Ivory Coast - Ghana basin of high Late Cretaceous accumulation rates, low rates in the early Cenozoic and high rates in the Late Cenozoic is also observed in other basins in the Equatorial Atlantic suggesting a discordance between the timing of uplift driven erosion and peaks in offshore accumulation (Ye, 2016). Ye (2016) conclude that the disagreement between the timing and magnitude of onshore denudation and the record of accumulation can be attributed to drainage reorganization and changes in size of paleocatchments and/or post-depositional sedimentary redistribution on sediment supply.

6. Conclusions

The landscape of the West African continental margin has largely evolved in response to thermal, tectonic, and surface processes since the emplacement of the Central Atlantic Magmatic Province in the Late Jurassic. This event marked the beginning of a series of tectonic events including rifting and continental break-up in the Central Atlantic followed by oblique movement and break-up in the Equatorial Atlantic. We infer the following from our new AFT data, thermal histories and their association with previously published AFT data.

(i) The thermal effect of the CAMP, either by direct heating or by burial under thick magmatic rocks, was significant across Guinea and Ivory Coast and sufficient to heat the presently exposed crust to temperatures > 110 °C. Further east, the absence of the CAMP facilitates preservation of older pre-rift AFT ages.
(ii) Patterns of AFT data with distance from the coast are comparable to those expected for traditional models of passive margin evolution, where most erosion occurs coastward of a continental divide during the main phase of rifting. Coastward limbs of long-wavelength flexural upwarps in Guinea and Ivory Coast were eroded, at moderate rates, in in response to the opening of the Central Atlantic in the Late Jurassic-Early Cretaceous and in response to the onset of transform movement in the Equatorial Atlantic during the early to mid-Cretaceous (145 – 90 Ma). Landward limbs, inland of the upwarp crest, also experienced suggest significant interior erosion that fed interior basins.
(iii) Fast cooling along the Ivory Coast coastline between ca. 130 and 110 Ma, is attributed to rapid erosion of a short-wavelength rift shoulder formed during the onset of transform faulting in the Equatorial Atlantic. The onset of fast cooling along the Guinean coast at 110–90 Ma is coeval with the timing of continental break-up in the Equatorial Atlantic. While some of the regional West African AFT data, particularly in Ghana, suggest fault reactivation of basement structures during the Cretaceous and potentially in the Early Cenozoic, it is poorly resolved elsewhere but remains possible
(iv) The AFT data and thermal histories infer low cooling rates and total amount of cooling through the Late Cretaceous and Cenozoic suggesting low erosion rates prevailed, which is consistent with Cenozoic denudation estimates of 2–10 m/Myr from Geomorphology studies. However, due to the lower temperature limit of the AFT thermochronometer, sub-km scale denudation cannot be confidently resolved. Similarly, burial of the coast and along the fringes of interior basins during the Late Cretaceous is a possibility but the total amount of heating related to this burial was < 60 °C

CRediT authorship contribution statement

M. Wildman: Data curation, Formal analysis, Investigation, Methodology, Validation, Visualization, Writing – original draft. **R. Brown:** Conceptualization, Data curation, Formal analysis, Investigation, Methodology, Resources, Supervision. **J. Ye:** Investigation, Methodology, Validation, Visualization, Writing – review & editing. **D. Chardon:** Conceptualization, Funding acquisition, Investigation, Methodology, Resources, Supervision, Validation, Writing – review & editing. **D. Rouby:** Conceptualization, Funding acquisition, Investigation, Methodology, Supervision, Validation, Writing – review & editing. **A.N. Kouamelan:** Methodology, Resources. **M. Dall'Asta:** Conceptualization, Funding acquisition, Investigation, Methodology, Project administration, Validation, Writing – review & editing.

Declaration of Competing Interest

The authors declare that they have no known competing financial interests or personal relationships that could have appeared to influence the work reported in this paper.

Acknowledgements

This study was funded by Total Energies R&D through the Transform Source-to-Sink Project (TS2P). We would like to thank David Mark Webster for assisting with sample collection and sample preparation during his PhD research and Robert McDonald for technical assistance at the University of Glasgow. We are indebted to the Direction Nationale de la Géologie (DNG) and particularly the late Nassirou Bah for facilitating fieldwork and sampling in Guinea. Frank Lisker and an anonymous reviewer are thanked for detailed comments on this work. This work is dedicated to the memory of our colleague and friend Roderick Brown, who sadly passed away shortly before this article was accepted. He will be sadly missed, and his legacy will continue.

Appendix A. Supplementary material

Supplementary data to this article can be found online at https://doi.org/10.1016/j.gr.2022.08.010.

References

Attoh, K., Brown, L., Haenlein, J., 2005. The role of Pan-African structures in intraplate seismicity near the termination of the Romanche fracture zone, West Africa. J. Afr. Earth. Sci. 43 (5), 549–555. https://doi.org/10.1016/j.jafrearsci.2005.09.006.

Attoh, K., Brown, L., Guo, J., Heanlein, J., 2004. Seismic stratigraphic record of transpression and uplift on the Romanche transform margin, offshore Ghana. Tectonophysics 378 (1–2), 1–16. https://doi.org/10.1016/j.tecto.2003.09.026.

Ault, A.K., Flowers, R.M., Bowring, S.A., 2013. Phanerozoic surface history of the Slave craton. Tectonics 32 (5), 1066–1083. https://doi.org/10.1002/tect.20069.

Balázs, A., Gerya, T., May, D., Tari, G., 2022. Contrasting transform and passive margin subsidence history and heat flow evolution: insights from 3D thermo-mechanical modelling. Geol. Soc. Spec. Publ. 524. https://doi.org/10.1144/SP524-2021-94.

Balestrieri, M.L., Stuart, F.M., Persano, C., Abbate, E., Bigazzi, G., 2005. Geomorphic development of the escarpment of the Eritrean margin, southern Red Sea from combined apatite fission-track and (U–Th)/He thermochronometry. Earth Planet. Sci. Lett. 231 (1–2), 97–110. https://doi.org/10.1016/j.epsl.2004.12.011.

Basile, C., 2015. Transform continental margins—Part 1: Concepts and models. Tectonophysics 661, 1–10. https://doi.org/10.1016/j.tecto.2015.08.034.

Basile, C., Mascle, J., Guiraud, R., 2005. Phanerozoic geological evolution of the Equatorial Atlantic domain. J. Afr. Earth. Sci. 43 (1–3), 275–282. https://doi.org/10.1016/j.jafrearsci.2005.07.011.

Beauvais, A., Chardon, D., 2013. Modes, tempo, and spatial variability of Cenozoic cratonic denudation: The West African example. Geochem., Geophy., Geosy. 14 (5), 1590–1608. https://doi.org/10.1002/ggge.20093.

Beauvais, A., Ruffet, G., Hénocque, O., Colin, F., 2008. Chemical and physical erosion rhythms of the West African Cenozoic morphogenesis: the 39Ar-40Ar dating of supergene K-Mn oxides. J. Geophys. Res.-Earth 113 (F4). https://doi.org/10.1029/2008JF000996.

Bennett, K.C., Rusk, D., 2002. Regional 2D seismic interpretation and exploration potential of offshore deepwater Sierra Leone and Liberia. West Africa. The Leading Edge 21 (11), 1118–1124. https://doi.org/10.1190/1.1523743.

Biari, Y., Klingelhoefer, F., Sahabi, M., Funck, T., Benabdellouahed, M., Schnabel, M., Reichert, C., Gutscherm, M.A., Bronner, A., Austin, J.A., 2017. Opening of the central Atlantic Ocean: implications for geometric rifting and asymmetric initial seafloor spreading after continental breakup. Tectonics 36 (6), 1129–1150. https://doi.org/10.1002/2017TC004596.

Bigot-Cormier, F., Basile, C., Poupeau, G., Bouillin, J.P., Labrin, E., 2005. Denudation of the Côte d'Ivoire-Ghana transform continental margin from apatite fission tracks. Terra Nova 17 (2), 189–195. https://doi.org/10.1111/j.1365-3121.2005.00605.x.

Braun, J., 2018. A review of numerical modeling studies of passive margin escarpments leading to a new analytical expression for the rate of escarpment migration velocity. Gondwana Res. 53, 209–224. https://doi.org/10.1016/j.gr.2017.04.012.

Brownfield, M. E., & Charpentier, R. R. (2003). Assessment of the undiscovered oil and gas of the Senegal Province, Mauritania, Senegal, the Gambia, and Guinea-Bissau, Northwest Africa., U.S. Geological Survey Bulletin 2207–A (2003), p. 28.

Buiter, S.J., Torsvik, T.H., 2014. A review of Wilson Cycle plate margins: A role for mantle plumes in continental break-up along sutures? Gondwana Res. 26 (2), 627–653. https://doi.org/10.1016/j.gr.2014.02.007.

Burke, K., 1996. The African plate. S. Afr. J. Geol. 99 (4), 341–409. https://doi.org/10.10520/EJC-942801f20.

Burke, K., Gunnell, Y., 2008. The African erosion surface: a continental-scale synthesis of geomorphology, tectonics, and environmental change over the past 180 million years. Geol. Soc. Am. Mem. 201, 66. https://doi.org/10.1130/2008.1201.

Campanile, D., Nambiar, C.G., Bishop, P., Widdowson, M., Brown, R., 2008. Sedimentation record in the Konkan-Kerala Basin: implications for the evolution of the Western Ghats and the Western Indian passive margin. Basin Res. 20 (1), 3–22. https://doi.org/10.1111/j.1365-2117.2007.00341.x.

Carlson, W.D., Donelick, R.A., Ketcham, R.A., 1999. Variability of apatite fission-track annealing kinetics: I. Experimental results. Am. Mineral. 84 (9), 1213–1223. https://doi.org/10.2138/am-1999-0901.

Chardon, D., Grimaud, J.L., Rouby, D., Beauvais, A., Christophoul, F., 2016. Stabilization of large drainage basins over geological time scales: Cenozoic West Africa, hot spot swell growth, and the Niger River. Geochem., Geophy., Geosy. 17 (3), 1164–1181. https://doi.org/10.1002/2015GC006169.

Chardon, D., Grimaud, J.-L., Beauvais, A., Bamba, O., 2018. West African lateritic pediments: landform-regolith evolution processes and mineral exploration pitfalls. Earth-Sci. Rev. 179, 124–146. https://doi.org/10.1016/j.earscirev.2018.02.009.

Clemson, J., Cartwright, J., Booth, J., 1997. Structural segmentation and the influence of basement structure on the Namibian passive margin. J Geol. Soc. London 154 (3), 477–482. https://doi.org/10.1144/gsjgs.154.3.0477.

Clift, P.D., Carter, A., Hurford, A.J., 1998. Apatite fission track analysis of Sites 959 and 960 on the transform continental margin of Ghana, West Africa, Proceedings of the Ocean Drilling Program, Scientific Results, Vol. 159, doi: 10.2973/odp.proc.sr.159.004.1998.

Cogné, N., Gallagher, K., Cobbold, P.R., 2011. Post-rift reactivation of the onshore margin of southeast Brazil: Evidence from apatite (U–Th)/He and fission-track data. Earth Planet. Sci. Lett. 309 (1–2), 118–130. https://doi.org/10.1016/j.epsl.2011.06.025.

Davison, I., 2005. Central Atlantic margin basins of North West Africa: geology and hydrocarbon potential (Morocco to Guinea). J. Afr. Earth. Sci. 43 (1–3), 254–274. https://doi.org/10.1016/j.jafrearsci.2005.07.018.

Deckart, K., Bertrand, H., Liégeois, J.P., 2005. Geochemistry and Sr, Nd, Pb isotopic composition of the Central Atlantic Magmatic Province (CAMP) in Guyana and Guinea. Lithos 82 (3–4), 289–314. https://doi.org/10.1016/j.lithos.2004.09.023.

De Grave, J., Glorie, S., Buslov, M.M., Izmer, A., Fournier-Carrie, A., Batalev, V.Y., Vanhaecke, F., Elburg, M., Van den haute, P., 2011. The thermo-tectonic history of the Song-Kul plateau, Kyrgyz Tien Shan: Constraints by apatite and titanite thermochronometry and zircon U/Pb dating. Gondwana Res. 20 (4), 745–763.

Deynoux, M., Affaton, P., Trompette, R., Villeneuve, M., 2006. Pan-African tectonic evolution and glacial events registered in Neoproterozoic to Cambrian cratonic and foreland basins of West Africa. J. Afr. Earth. Sci. 46 (5), 397–426. https://doi.org/10.1016/j.jafrearsci.2006.08.005.

Donelick, R.A., O'Sullivan, P.B., Ketcham, R.A., 2005. Apatite fission-track analysis. Rev. Mineral. Geochem. 58 (1), 49–94. https://doi.org/10.2138/rmg.2005.58.3.

Ennih, N., Liégeois, J.P., 2008. The boundaries of the West African craton, with special reference to the basement of the Moroccan metacratonic Anti-Atlas belt. Geol. Soc. Spec. Publ. 297 (1), 1–17. https://doi.org/10.1144/SP297.1.

Fernie, N., Glorie, S., Jessell, M.W., Collins, A.S., 2018. Thermochronological insights into reactivation of a continental shear zone in response to Equatorial Atlantic rifting (northern Ghana). Sci. Rep. 8 (1), 1–14. https://doi.org/10.1038/s41598-018-34769-x.

Gallagher, K., 2012. Transdimensional inverse thermal history modeling for quantitative thermochronology. J. Geopys. Res.-Sol. Ea. 117 (B2), n/a–n/a.

Gallagher, K., Brown, R., 1997. The onshore record of passive margin evolution. J Geol. Soc. London 154 (3), 451–457. https://doi.org/10.1144/gsjgs.154.3.0451.

Gallagher, K., Brown, R., 1999. Denudation and uplift at passive margins: the record on the Atlantic Margin of southern Africa. Philos. Trans. R. Soc. Series A: Math. Phys. Eng. Sci. 357 (1753), 835–859.

Gibson, G.M., Totterdell, J.M., White, L.T., Mitchell, C.H., Stacey, A.R., Morse, M.P., Whitaker, A., 2013. Pre-existing basement structure and its influence on continental rifting and fracture zone development along Australia's southern rifted margin. J Geol. Soc. London 170 (2), 365–377. https://doi.org/10.1144/jgs2012-040.

Gilchrist, A.R., Summerfield, M.A., 1990. Differential denudation and flexural isostasy in formation of rifted-margin upwarps. Nature 346 (6286), 739–742. https://doi.org/10.1038/346739a0.

Gleadow, A.J.W., Lovering, J.F., 1978. Thermal history of granitic rocks from western Victoria: A fission-track dating study. J Geol. Soc. Aust. 25 (5–6), 323–340. https://doi.org/10.1080/00167617808729039.

Gleadow, A.J., Duddy, I.R., Green, P.F., Hegarty, K.A., 1986. Fission track lengths in the apatite annealing zone and the interpretation of mixed ages. Earth Planet. Sci. Lett. 78 (2–3), 245–254.

Green, P.F., 1986. On the thermo-tectonic evolution of Northern England: Evidence from fission track analysis. Geol. Mag. 123, 493–506. https://doi.org/10.1017/S0016756800035081.

Greenroyd, C.J., Peirce, C., Rodger, M., Watts, A.B., Hobbs, R.W., 2008. Demerara plateau—The structure and evolution of a transform passive margin. Geophys. J. Int. 172 (2), 549–564. https://doi.org/10.1111/j.1365-246X.2007.03662.x.

Grimaud, J.L., Chardon, D., Beauvais, A., 2014. Very long-term incision dynamics of big rivers. Earth Planet. Sci. Lett. 405, 74–84. https://doi.org/10.1016/j.epsl.2014.08.021.

Grimaud, J.L., Rouby, D., Chardon, D., Beauvais, A., 2018. Cenozoic sediment budget of West Africa and the Niger delta. Basin Res. 30 (2), 169–186. https://doi.org/10.1111/bre.12248.

Guiraud, R., Bosworth, W., Thierry, J., Delplanque, A., 2005. Phanerozoic geological evolution of Northern and Central Africa: an overview. J. Afr. Earth. Sci. 43 (1–3), 83–143. https://doi.org/10.1016/j.jafrearsci.2005.07.017.

Gunnell, Y., 2003. Radiometric ages of laterites and constraints on long-term denudation rates in West Africa. Geology 31 (2), 131–134. https://doi.org/10.1130/0091-7613(2003)031<0131:RAOLAC>2.0.CO;2.

Heine, C., Zoethout, J., Müller, R.D., 2013. Kinematics of the South Atlantic rift. Solid Earth 4, 215–253. https://doi.org/10.5194/se-4-215-2013.

Hubbard, F.H., 1983. The Phanerozoic cover sequences preserved as xenoliths in the kimberlite of eastern Sierra Leone. Geol. Mag. 120 (1), 67–71. https://doi.org/10.1017/S0016756800025048.

Hurford, A.J., Green, P.F., 1983. The zeta age calibration of fission-track dating. Chem. Geol. 41, 285–317. https://doi.org/10.1016/S0009-2541(83)80026-6.

Ketcham, R.A., Carter, A., Donelick, R.A., Barbarand, J., Hurford, A.J., 2007. Improved modeling of fission-track annealing in apatite. Am. Mineral. 92 (5–6), 799–810. https://doi.org/10.2138/am.2007.2281.

Ketcham, R.A., van der Beek, P., Barbarand, J., Bernet, M., Gautheron, C., 2018. Reproducibility of thermal history reconstruction from apatite fission-track and (U-Th)/He data. Geochem., Geophy., Geosy. 19 (8), 2411–2436. https://doi.org/10.1029/2018GC007555.

Ksienzyk, A.K., Dunkl, I., Jacobs, J., Fossen, H., Kohlmann, F., 2014. From orogen to passive margin: constraints from fission track and (U–Th)/He analyses on Mesozoic uplift and fault reactivation in SW Norway. Geol. Soc. Spec. Publ. 390 (1), 679–702. https://doi.org/10.1144/SP390.27.

Labails, C., Olivet, J.L., Aslanian, D., Roest, W.R., 2010. An alternative early opening scenario for the Central Atlantic Ocean. Earth Planet. Sci. Lett. 297 (3–4), 355–368. https://doi.org/10.1016/j.epsl.2010.06.024.

Lisker, F., T. John, and B. Ventura. (2008). Denudation and uplift across the Ghana transform margin as indicated by new apatite fission track data, In. Katlenburg-Lindau: Katlenburg-Lindau, Germany: Copernicus GmbH on behalf of the European Geosciences Union (EGU).

Lodhia, B.H., Roberts, G.G., Fraser, A.J., Jarvis, J., Newton, R., Cowan, R.J., 2019. Observation and Simulation of Solid Sedimentary Flux. Examples From Northwest Africa. Geochem., Geophy., Geosy. 20 (11), 4613–4634. https://doi.org/10.1029/2019GC008262.

Lompo, M., 2010. Paleoproterozoic structural evolution of the Man-Leo Shield (West Africa). Key structures for vertical to transcurrent tectonics. J. Afr. Earth. Sci. 58 (1), 19–36. https://doi.org/10.1016/j.jafrearsci.2010.01.005.

Loncke, L., Roest, W. R., Klingelhoefer, F., C. Basile, Graindorge, D., Heuret, A., Marcaillou, B., Museur, T., Fanget, A. S., & Mercier de Lépinay, M. (2020) Transform marginal plateaus, Earth Sci. Rev. 203, 102940 (32 p.), doi: 10.1016/j.earscirev.2019.102940.

Łuszczak, K., Persano, C., Braun, J., Stuart, F.M., 2017. How local crustal thermal properties influence the amount of denudation derived from low-temperature thermochronometry. Geology 45 (9), 779–782. https://doi.org/10.1130/G39036.1.

Marzoli, A., Bertrand, H., Knight, K.B., Cirilli, S., Buratti, N., Vérati, C., Nomade, S., Renne, P.R., Youbi, N., Martini, R., Allenbach, K., Neuwerth, R., Rapaille, C., Zaninetti, L., Bellieni, G., 2004. Synchrony of the Central Atlantic magmatic province and the Triassic-Jurassic boundary climatic and biotic crisis. Geology 32 (11), 973–976. https://doi.org/10.1016/j.palaeo.2006.06.035.

Marzoli, A., Callegaro, S., Dal Corso, J., Davies, J.H., Chiaradia, M., Youbi, N., Bertrand, H., Reisberg, L., Merle, R., Jourdan, F., 2018. The Central Atlantic magmatic province (CAMP): a review. In: The Late Triassic World. Springer, Cham, pp. 91–125. https://doi.org/10.1007/978-3-319-68009-5_4.

McHone, J.G., 2003. Volatile emissions from Central Atlantic Magmatic Province basalts: Mass assumptions and environmental consequences. Geoph. Monog. Series 136, 241–254. https://doi.org/10.1029/136GM013.

Mercier de Lépinay, M., Loncke, L., Basile, C., Roest, W.R., Patriat, M., Maillard, A., De Clarens, P., 2016. Transform continental margins–Part 2: A worldwide review. Tectonophysics 693, 96–115. https://doi.org/10.1016/j.tecto.2016.05.038.

Moulin, M., Aslanian, D., Unternehr, P., 2010. A new starting point for the South and Equatorial Atlantic Ocean. Earth Sci. Rev. 98 (1–2), 1–37. https://doi.org/10.1016/j.earscirev.2009.08.001.

Nemcok, M., Rybar, S., Sinha, S. T., Hermeston, S. A., & Ledvenyiova, L. (Eds.). (2016, September). Transform Margins: Development, Controls and Petroleum Systems. Geological Society of London, doi: 10.6084/m9.figshare.c.3276407.

Nomade, S., Knight, K.B., Beutel, E., Renne, P.R., Verati, C., Féraud, G., Marzoli, A., Youbi, N., Bertrand, H., 2007. Chronology of the Central Atlantic Magmatic Province: implications for the Central Atlantic rifting processes and the Triassic-Jurassic biotic crisis. Palaeogeogr. Palaeoclimatol. Palaeoecol. 244 (1–4), 326–344. https://doi.org/10.1016/j.palaeo.2006.06.034.

Peace, A., McCaffrey, K., Imber, J., van Hunen, J., Hobbs, R., Wilson, R., 2018. The role of pre-existing structures during rifting, continental breakup and transform system development, offshore West Greenland. Basin Res. 30 (3), 373–394. https://doi.org/10.1111/bre.12257.

Persano, C., Stuart, F.M., Bishop, P., Barfod, D.N., 2002. Apatite (U–Th)/He age constraints on the development of the Great Escarpment on the southeastern Australian passive margin. Earth Planet. Sci. Lett. 200 (1–2), 79–90. https://doi.org/10.1016/S0012-821X(02)00614-3.

Peulvast, J.P., Sales, V.C., Bétard, F., Gunnell, Y., 2008. Low post-Cenomanian denudation depths across the Brazilian Northeast: implications for long-term landscape evolution at a transform continental margin. Global Planet. Change 62 (1–2), 39–60. https://doi.org/10.1016/j.gloplacha.2007.11.005.

Rollinson, H., 2016. Archaean crustal evolution in West Africa: A new synthesis of the Archaean geology in Sierra Leone, Liberia. Guinea and Ivory Coast. Precambrian Res. 281, 1–12. https://doi.org/10.1016/j.precamres.2016.05.005.

Séranne, M., Anka, Z., 2005. South Atlantic continental margins of Africa: a comparison of the tectonic vs climate interplay on the evolution of equatorial west Africa and SW Africa margins. J. Afr. Earth. Sci. 43 (1–3), 283–300. https://doi.org/10.1016/j.jafrearsci.2005.07.010.

Spotila, J.A., Bank, G.C., Reiners, P.W., Naeser, C.W., Naeser, N.D., Henika, B.S., 2004. Origin of the Blue Ridge escarpment along the passive margin of Eastern North America. Basin Res. 16 (1), 41–63. https://doi.org/10.1111/j.1365-2117.2003.00219.x.

Stanley, J.R., Flowers, R.M., Bell, D.R., 2015. Erosion patterns and mantle sources of topographic change across the southern African Plateau derived from the shallow and deep records of kimberlites. Geochem., Geophy., Geosy. 16 (9), 3235–3256. https://doi.org/10.1002/2015GC005969.

Summerfield, M.A., 2000. Geomorphology and Global Tectonics. Wiley, Chichester (386 pp.).

Svensen, H.H., Torsvik, T.H., Callegaro, S., Augland, L., Heimdal, T.H., Jerram, D.A., Planke, S., Pereira, E., 2018. Gondwana Large Igneous Provinces: plate reconstructions, volcanic basins and sill volumes. Geol. Soc. Spec. Publ. 463 (1), 17–40. https://doi.org/10.1144/sp463.7.

Tari, G., 2006. Traditional and new play types of the offshore Tano Basin of Cote D'Ivoire and Ghana. West Africa. Houston Geological Society Bulletin 48 (5), 27–30.

Traoré, K., Chardon, D., Naba, S., Wane, O., Bouaré, M.L., 2022. Paleoproterozoic collision tectonics in West Africa: Insights into the geodynamics of continental growth. Precambr. Res. 376, 106692.

Van Ranst, G., Pedrosa-Soares, A.C., Novo, T., Vermeesch, P., De Grave, J., 2020. New insights from low-temperature thermochronology into the tectonic and geomorphologic evolution of the south-eastern Brazilian highlands and passive margin. Geosci. Front. 11 (1), 303–324. https://doi.org/10.1016/j.gsf.2019.05.011.

Vasconcelos, P.M., Brimhall, G.H., Becker, T.A., Renne, P.R., 1994. 40Ar39Ar analysis of supergene jarosite and alunite: Implications to the paleoweathering history of the western USA and West Africa. Geochim. Cosmochim. Ac. 58 (1), 401–420. https://doi.org/10.1016/0016-7037(94)90473-1.

Vermeesch, P., 2021. On the treatment of discordant detrital zircon U-Pb data. Geochronology 3 (1), 247–257. https://doi.org/10.5194/gchron-3-247-2021.

Villeneuve, M., 2005. Paleozoic basins in West Africa and the Mauritanide thrust belt. J. Afr. Earth. Sci. 43 (1–3), 166–195. https://doi.org/10.1016/j.jafrearsci.2005.07.012.

Villeneuve, M., 2008. Review of the orogenic belts on the western side of the West African craton: the Bassarides, Rokelides and Mauritanides. Geol. Soc. Spec. Publ. 297 (1), 169–201. https://doi.org/10.1144/sp297.8.

Villeneuve, M., Cornée, J.J., 1994. Structure, evolution and palaeogeography of the West African craton and bordering belts during the Neoproterozoic. Precambrian Res. 69 (1–4), 307–326. https://doi.org/10.1016/0301-9268(94)90094-9.

Wildman, M., Brown, R., Beucher, R., Persano, C., Stuart, F., Gallagher, K., Schwanethal, J., Carter, A., 2016. The chronology and tectonic style of landscape evolution along the elevated Atlantic continental margin of South Africa resolved by joint apatite fission track and (U-Th-Sm)/He thermochronology. Tectonics 35 (3), 511–545. https://doi.org/10.1002/2015TC004042).

Wildman, M., Cogné, N., & Beucher, R. (2020). Fission-track thermochronology applied to the evolution of passive continental margins. In Fission-Track Thermochronology and its Application to Geology (pp. 351-371). Springer, Cham., 10.1007/978-3-319-89421-8_20.

Wildman, M., Webster, D., Brown, R., Chardon, D., Rouby, D., Ye, J., Huyghe, D., Dall'Asta, M., 2019. Long-term evolution of the West African transform margin: estimates of denudation from Benin using apatite thermochronology. J Geol. Soc. London 176 (1), 97–114. https://doi.org/10.1144/jgs2018-078.

Withjack, M.O., Schlische, R.W., Olsen, P.E., 2012. Development of the passive margin of eastern North America: Mesozoic rifting, igneous activity, and breakup. In: Roberts, D.G., Bally, A.W. (Eds.), Regional Geology and Tectonics. Phanerozoic Rift Systems and Sedimentary Basins, Elsevier, New York, pp. 301–335. https://doi.org/10.1016/B978-0-444-56356-9.00012-2.

Ye, J., Chardon, D., Rouby, D., Guillocheau, F., Dall'asta, M., Ferry, J. N., & Broucke, O. (2017). Paleogeographic and structural evolution of northwestern Africa and its Atlantic margins since the early Mesozoic. Geosphere, 13(4), 1254-1284, doi: 10.1130/GES01426.1.

Ye, J., Rouby, D., Chardon, D., Dall'asta, M., Guillocheau, F., Robin, C., Ferry, J.N., 2019. Post-rift stratigraphic architectures along the African margin of the Equatorial Atlantic: Part I the influence of extension obliquity. Tectonophysics 753, 49–62. https://doi.org/10.1016/j.tecto.2019.01.003.

Ye, J., 2016. Evolution topographique, tectonique et sédimentaire syn- à post-rift de la marge transformante ouest Africaine. GET Toulouse, PhD Thesis, 273 p.